NOVA SCHOOL OF SCIENCE & TECHNOLOGY

DEPARTMENT OF ELECTRICAL AND COMPUTER ENGINEERING

RAFAEL FERNANDES TEIXEIRA

BSc in Electrical and Computer Engineering

DESIGN OF LOW-COMPLEXITY CHANNEL ESTIMATION TECHNIQUES FOR LARGE MIMO SYSTEMS

MASTER IN ELECTRICAL AND COMPUTER ENGINEERING

NOVA University Lisbon
March, 2023

NOVA SCHOOL OF
SCIENCE & TECHNOLOGY

DEPARTMENT OF ELECTRICAL
AND COMPUTER ENGINEERING

DESIGN OF LOW-COMPLEXITY CHANNEL ESTIMATION TECHNIQUES FOR LARGE MIMO SYSTEMS

RAFAEL FERNANDES TEIXEIRA

BSc in Electrical and Computer Engineering

Adviser: João Francisco Martinho Lêdo Guerreiro
Assistant Professor, NOVA University Lisbon

Co-adviser: Rui Miguel Henriques Dias Morgado Dinis
Associate Professor with Habilitation, NOVA University Lisbon

MASTER IN ELECTRICAL AND COMPUTER ENGINEERING

NOVA University Lisbon
March, 2023

Design of Low-Complexity Channel Estimation Techniques for Large MIMO Systems

This document was created with the (pdf/Xe/Lua)LaTeX processor and the NOVAthesis template (v6.9.4) [26].

This dissertation is dedicated to my dear parents and brother.
For their endless love, support and encouragement.

Acknowledgements

First and foremost, I would like to express my gratitude and appreciation to my advisors Professor João Guerreiro and Professor Rui Dinis, for their consistent support, guidance and scientific knowledge throughout the realization of this thesis. Furthermore, I am also thankful to the NOVA School of Science & Technology and its entire member's staff for all the considerate guidance. Last but not least, I am forever grateful to my family and friends for all their unconditional love and support and without whom I would not have made it through my master's degree.

"As for the future, your task is not to foresee it, but to enable it." (Antoine de Saint Exupéry)

Abstract

In recent years, a fast and considerable improvement in the field of wireless communication systems has been observed. This is explained not only by a continuous rise of users and Internet of Things (IoT) devices but also by the demanding applications that each user requires. Moreover, it is foreseen that this trend will continue to be observed in the next years.

In the physical layer of wireless communication systems, Massive MIMO (mMIMO) is today's most promising antenna technology. However, there is still much to be improved in the prospective future, not only to enhance and tackle the limitations of mMIMO but also regarding the development and evolution of new smart antenna technologies with Extremely Large Antenna Arrays (ELAAs) for the upcoming Sixth Generation (6G), namely Large Intelligent Surface (LIS), Radio Stripe (RS) and Intelligent Reflective Surface (IRS). Theoretically, these new antenna technologies allow for huge spectral efficiency gains and high Quality of Service (QoS) while serving a huge number of users. However, besides the potentialities of the new ELAAs systems, there is a set of important challenges that need to be addressed, among which accurate channel models, channel estimation algorithms, and low-complexity implementations are considered to be the most important.

The main goal of this dissertation is to develop low-complexity channel estimation techniques that can be used by systems with a very large number of antennas without leading to large overhead and computational costs. In that sense, two simplified channel estimation techniques are proposed for large MIMO systems, one involving spatial information such as the array geometry and the angles of arrival and another based on the spatial interpolation of the channel. Results of the performance of both techniques are presented and it is demonstrated that both techniques can be used to simplify channel estimation in large MIMO systems.

Keywords: LIS, RS, IRS, mMIMO, wireless communications, channel modeling & estimation, 6G.

Resumo

Nos últimos anos observou-se uma evolução rápida e considerável nos sistemas de comunicação sem fios. Isto é explicado, não só por um aumento contínuo de utilizadores e dispositivos Internet of Things (IoT), mas também pelas aplicações cada vez mais exigentes que cada utilizador necessita. Além disso, prevê-se que esta tendência se mantenha nos próximos anos.

Na camada física dos sistemas de comunicação sem fios, Massive MIMO (mMIMO) é hoje a tecnologia de antenas mais promissora. No entanto, existe ainda muito a melhorar no futuro, não só nos sistemas mMIMO, mas também no desenvolvimento de novas tecnologias de antenas inteligentes com Extremely Large Antenna Arrays (ELAAs) para a futura Sixth Generation (6G), nomeadamente Large Intelligent Surface (LIS), Radio Stripe (RS) e Intelligent Reflective Surface (IRS). Teoricamente, estas novas tecnologias de antenas permitem enormes ganhos de eficiência espectral e elevada Quality of Service (QoS), servindo ao mesmo tempo um enorme número de utilizadores. Contudo, para além dos vários potenciais dos novos sistemas de ELAAs, existe um conjunto de importantes desafios que precisam de ser abordados, entre os quais modelos de canais precisos, algoritmos de estimação de canais e implementações de baixa complexidade são considerados como sendo os mais importantes.

O objetivo principal desta dissertação é desenvolver técnicas de estimativa de canais de baixa complexidade que possam ser usadas por sistemas com elevado número de antenas sem levar à existência de um *overhead* considerável ou custos computacionais acrescidos. Nesse sentido, são propostas duas técnicas simplificadas de estimativa de canais para sistemas MIMO de grande dimensão, uma envolvendo informação espacial como a geometria do *array* e os ângulos de chegada e outra baseada na interpolação espacial do canal. Os resultados do desempenho de ambas as técnicas são apresentados e é demonstrado que ambas as técnicas podem ser utilizadas para simplificar a estimativa de canais em sistemas multi-antenas MIMO de grande dimensão.

Palavras-chave: LIS, RS, IRS, mMIMO, comunicações sem fios, modelação e estimativa de canal, 6G.

Contents

List of Figures x

List of Tables xiii

Acronyms xv

Symbols xvii

1 Introduction 1
- 1.1 Motivation . . . 1
- 1.2 Objectives and Contributions . . . 3
- 1.3 Document Structure . . . 3

2 State-of-the-Art 5
- 2.1 Multiple-Input Multiple-Output (MIMO) Systems . . . 5
  - 2.1.1 Advantages of MIMO systems . . . 5
  - 2.1.2 Types of MIMO Systems . . . 6
- 2.2 Extremely Large Antenna Array (ELAA) Systems . . . 8
  - 2.2.1 Large Intelligent Surface (LIS) . . . 8
  - 2.2.2 Cell-Free mMIMO & Radio Stripes (RS) . . . 9
  - 2.2.3 Intelligent Reflective Surface (IRS) . . . 10
- 2.3 Challenges of Communication Systems Based on ELAAs . . . 11
  - 2.3.1 Channel Modeling . . . 12
  - 2.3.2 Channel Estimation . . . 15
  - 2.3.3 Other Issues . . . 19

3 Low-complexity Channel Estimation using Spatial Information 20
- 3.1 System Characterization & Channel Modeling . . . 20
- 3.2 Low-complexity Channel Estimation Algorithm based on the Angles of Arrival (AoA) . . . 25
- 3.3 Performance Results . . . 30

3.3.1 Line-of-Sight (LoS) Communication Environment 32
3.3.2 Scattering Communication Environment 38
3.3.3 Final Remarks & Results Discussion 41

4 Low-Complexity Channel Estimation using Spatial Interpolation **42**
4.1 System Characterization 42
4.2 Estimation of the Channel Gain using Discrete Fourier Transform (DFT) 44
4.2.1 Channel Gain and Fourier Transform (FT) 44
4.2.2 Nyquist Sampling Theorem 46
4.3 Performance Results 48
4.3.1 Channel Gain 49
4.3.2 Channel Gain Estimation with Different Sampling Ratios 51
4.3.3 Final Remarks & Results Discussion 57

5 Conclusions **58**

Bibliography **61**

List of Figures

1.1 Global mobile subscriber growth. 2
1.2 Global mobile M2M growth. 2

2.1 Representation of Point-to-Point MIMO system. 6
2.2 Representation of Multi-User MIMO system. 7
2.3 Representation of a LIS scenario with multi-user communication. 9
2.4 Ericsson RS prototype. 10
2.5 Representation of a IRS system communication. 11
2.6 Visual representation of the differences between the near-field and the far-field regions. 13
2.7 Visual representation of the TDD and FDD modes. 16
2.8 Representation of the pilot contamination effects. 17

3.1 Representation of the LIS (in green) in the ceiling of an indoor room from two different viewing angles. 21
3.2 Representation of the scattering communication environment between one user and the LIS (in green) in an indoor room. 22
3.3 Illustrative representation of the images method used for ray tracing. . . . 23
3.4 Representation of the LIS divided into panels and the respective antenna elements of each panel. 26
3.5 Illustrative representation of the AoA - azimuth (φ_{ref}) and elevation (θ_{ref}). 28
3.6 Illustration of variables d_x and d_y that represent the relative distance between the reference antenna and another antenna of a given panel. 29
3.7 Indoor room scattering communication scenario with two users ($User\ 1$ and $User\ 2$) with randomly generated positions and the LIS at $z = 3$ m. 30
3.8 NMSE measurements for each antenna in a LIS panel. 31
3.9 Indoor room LoS communication scenario with one user at $z = 1$ m centered with the LIS, which is at $z = 10$ m. 32
3.10 NMSE measurements for each antenna in a LIS regarding the scenario depicted in figure 3.9. 33

3.11 NMSE measurements for each antenna in a LIS regarding the scenario depicted in figure 3.9 except now with the user at $z = 9$ m. 33
3.12 Indoor room LoS communication scenario with one user at $z = 1$ m centered with the LIS, which is at $z = 3$ m. 34
3.13 NMSE measurements for each antenna in a LIS, considering only a LoS communication scenario with one user at $z = 1$ m, centered with the LIS positioned at $z = 3$ m and with $M = 100$ total antennas. 35
3.14 NMSE measurements for each antenna in a LIS, considering only a LoS communication scenario with one user at $z = 1$ m, centered with the LIS positioned at $z = 3$ m and with $M = 400$ total antennas. 35
3.15 NMSE measurements for each antenna in a LIS, considering only a LoS communication scenario with one user at $z = 1$ m, centered with the LIS positioned at $z = 3$ m and divided by $P = 4$ panels, each with $a_p = 100$ antennas, totalling $M = 400$ antennas. 36
3.16 Representation of the LIS divided in $P = 16$ panels. 36
3.17 NMSE measurements for each antenna in a LIS, considering only a LoS communication scenario with one user at $z = 1$ m, centered with the LIS positioned at $z = 3$ m and divided by $P = 16$ panels, each with $a_p = 25$ antennas, totalling $M = 400$ antennas. 37
3.18 Indoor room scattering communication scenario with one user at $z = 1$ m centered with the LIS, which is at $z = 3$ m. 38
3.19 NMSE measurements for each antenna in a LIS, considering a scattering communication scenario with one user at $z = 1$ m, centered with the LIS positioned at $z = 3$ m and with $M = 100$ total antennas. 39
3.20 NMSE measurements for each antenna in a LIS, considering a scattering communication scenario with one user at $z = 1$ m, centered with the LIS positioned at $z = 3$ m and with $M = 400$ total antennas. 39
3.21 NMSE measurements for each antenna in a LIS, considering a scattering communication scenario with one user at $z = 1$ m, centered with the LIS positioned at $z = 3$ m and divided by $P = 4$ panels, each with $a_p = 100$ antennas, totalling $M = 400$ antennas. 40
3.22 NMSE measurements for each antenna in a LIS, considering a scattering communication scenario with one user at $z = 1$ m, centered with the LIS positioned at $z = 3$ m and divided by $P = 16$ panels, each with $a_p = 25$ antennas, totalling $M = 400$ antennas. 40

4.1 Illustrative representation of the conceptualized RS communication scenario. 43
4.2 Illustrative representation of a RS with $N = 12$ antennas and the respective variables l_{RS}, d_x, d_s and S used in the proposed method. In this case, $S = 4$ and therefore, $N_s = 3$. 48

4.3 Evolution of the channel gain along a limitless RS with $U = 2$ users located in different positions. 49
4.4 Spatial frequency-domain channel gain considering $U = 2$ users located in different positions. 50
4.5 Communication scenario where a RS with $l_{RS} = 10$ m serving $U = 3$ users located in different positions (on the left figure) and evolution of the channel gain for each respective users (on the right figure). 51
4.6 Communication scenario where a RS with $l_{RS} = 10$ m serving $U = 3$ users located in different positions and aligned vertically (on the left figure); and evolution of the channel gain for each respective users (on the right figure). 52
4.7 Communication scenario where a RS with $l_{RS} = 10$ m serving $U = 3$ users located in different positions and aligned horizontally (on the left figure); and evolution of the channel gain for each respective users (on the right figure). 53
4.8 Representation of the channel gain evolution along the RS for a user positioned at $(x_u, y_u) = (5, 5)$ considering different sampling ratios S. 53
4.9 Representation of the channel gain evolution along the RS for a user positioned at $(x_u, y_u) = (5, 10)$ considering different sampling ratios S. 54
4.10 Representation of the channel gain evolution along the RS for a user positioned at $(x_u, y_u) = (10, 10)$ considering different sampling ratios S. 54
4.11 Representation of the channel gain evolution along the RS for a user positioned at $(x_u, y_u) = (10, 2)$ considering different sampling ratios S. 55
4.12 Illustrative representation of a communication scenario in which the RS communicates with users positioned in a grid. 55
4.13 MSE measurements of the channel gains estimates considering different values of S. 56

List of Tables

3.1 Parameters associated with the design of the LIS and the communication environment. 27

4.1 Parameters associated with the design of the RS and the communication environment. 43

Acronyms

5G Fifth Generation 1, 5, 7–9, 16
6G Sixth Generation vi, vii, 1–5, 8, 16, 17, 58

AoA Angle of Arrival x, 3, 4, 12–14, 17, 20, 21, 25, 27, 28, 31, 32, 41, 59
AP Access Point 1, 9, 10

BS Base Station 1, 6–8, 15–17, 58

CAGR Compound Annual Growth Rate 2
CFR Channel Frequency Response 12, 20, 24
CIR Channel Impulsive Response 12, 20, 21, 24, 28, 32, 41, 57, 59, 60
CPU Central Processing Unit 9, 10, 19
CSI Channel State Information 15, 16

DFT Discrete Fourier Transform 44, 47, 48, 57, 59
DoF Degrees of Freedom 5

ELAA Extremely Large Antenna Array vi, vii, 2–5, 8, 11–15, 18–20, 25, 42, 57–60

FDD Frequency Division Duplexing x, 15, 16
FT Fourier Transform 3, 12, 45, 46, 49

HWI Hardware Impairments 19

IDFT Inverse Discrete Fourier Transform 48
IoT Internet of Things vi, vii, 1, 9
IRS Intelligent Reflective Surface vi, vii, x, 5, 10, 11, 58

LIS Large Intelligent Surface vi, vii, x, xi, xiii, 3, 5, 8, 9, 12–15, 19–23, 25–27, 30–42, 58, 59
LoS Line-of-Sight x, xi, 8, 11, 14, 15, 19, 21, 22, 32, 34–38, 41, 42, 44
LS Least Square 17, 18
LTI Linear Time-Invariant 23

M2M Machine-To-Machine x, 1, 2
MIMO Multiple-Input Multiple-Output vi, vii, 1, 5–8, 12, 25, 58
mMIMO Massive MIMO vi, vii, 1–3, 5, 7–9, 11–19, 25, 58
MMSE Minimum Mean Squared Error 17, 18
MSE Mean Squared Error xii, 17, 48, 52, 56
MU-MIMO Multi-user MIMO 6–8, 15

NLoS Non-Line-of-Sight 19
NMSE Normalized Mean Squared Error x, xi, 29, 31–41, 59

PA Power Amplifier 7
PP-MIMO Point-to-Point MIMO 6
PSD Power Spectral Density 46, 57, 60

QoS Quality of Service vi, vii, 8, 9, 11

RS Radio Stripe vi, vii, x–xiii, 3, 5, 9, 10, 12, 15, 42–60
RSS Received Signal Strength 19
RX Receive 5, 6, 12–15, 23, 58

SE Spectral Efficiency 1, 5, 8, 9, 13, 15
SNR Signal-to-Noise Ratio 5, 6, 8, 9, 11
SPU Signal Processing Unit 9, 10, 19

TDD Time Division Duplexing x, 15, 16, 19
TX Transmit 5, 6, 12, 15, 23, 58

UE User Equipment 3, 5–10, 12–21, 25, 41, 42, 58–60

Symbols

A_{ir}	Area of the indoor room 27, 30
A_{LIS}	Area of the LIS 26, 27
a_p	Total number of antennas per panel in the LIS xi, 26, 27, 30, 34, 36–38, 40
a_{ps}	Number of antennas per each panel side of the LIS 26, 27
$\alpha^{(r,u,i)}$	Complex amplitude to a given ray 24, 25, 29
$\varphi_{ref}^{(p,u,i)}$	Azimuth angle associated to a reference antenna 27–29
β_i	Fading component associated to a given ray 24
c	Speed of Light in Vacuum 20, 24, 42, 43
D	Distance between antenna elements in a LIS 26–28, 30
$d^{(r,u,i)}$	Distance travelled by the ith ray associated to uth to the antenna r 22–24
d_s	Distance between sampling antennas xi, 47, 48
$d_u(x)$	Distance associated with the LoS ray between the user and a given antenna in the RS 44, 45
d_x	Distance between antenna elements in the RS xi, 42, 43, 47, 48, 50, 51
$\tau^{(r,u,i)}$	Delay associated to a given ray 24, 25
$\Delta_d^{(p,r,u,i)}$	Difference in the propagation distance between the uth user and the rth antenna with respect to the reference antenna of a panel 28, 29
$\Delta_\varphi^{(p,r,u,i)}$	Phase difference between the reference antenna of a panel and the rth antenna of the same panel 29
$\theta_{ref}^{(p,u,i)}$	Elevation angle associated to a reference antenna 27, 28
f_c	Carrier Wave Frequency 20, 27, 30, 42, 43
f_s	Sampling frequency 46, 47

$G_P(\nu)$	"Discrete-space" Fourier transform 46
$G_u(\nu)$	Fourier transform of $g_u(x)$ 46, 49
$g_u(x)$	Channel Gain 44, 45, 49, 50
$\hat{\mathbf{g}}_{u,a}$	Vector composed by the estimated channel gains 48
$\mathbf{G}_{u,s}$	DFT of $\mathbf{g}_{u,s}$ 48
$\mathbf{g}_{u,s}$	Vector composed by the channel gains of the N_s antennas 47, 48
Γ_i	Reflection coefficient associated to the ith wall reflection 24
$H(f)^{(r,u)}$	CFR between the rth antenna and the uth user 25
$h(t)^{(r,u)}$	CIR between the rth antenna and the uth user 24
$\hat{\alpha}^{(p,r,u,i)}$	Estimated complex amplitude of a given ray 29
I	Number of rays associated to an user 21, 22, 27, 38
l_{LIS}	Length of the LIS side 26, 27
l_{RS}	Length of the RS xi, xii, 42, 43, 47–53
λ	Wavelength 12, 20, 23, 24, 26, 27, 29, 30, 42–45, 50, 51
M	Total number of antennas in the LIS xi, 26, 27, 30, 34–40
N	Total number of antennas in the RS xi, 42, 43, 47, 48, 50, 51
N_s	Number of sample antennas xi, 47, 48
P	Number of panels in the LIS xi, 26, 27, 30, 34, 36–38, 40
P_{rx}	Received power 24, 44, 45
P_{tx}	Transmit power 20, 24, 27, 44, 45
P_u	Total power of $G_u(\nu)$ 46
S	Sampling ratio xi, xii, 47, 48, 51–56
$\theta_u(x)$	Channel phase associated to the propagation delay 44
$\tilde{\alpha}_u(x)$	Baseband complex-valued LoS ray that defines the link between the user and an antenna in the RS 44
$\mathbf{g}_{u,a}$	Vector composed by the channel gains of the N total antennas 48
U	Number of users xii, 20, 21, 27, 42, 43, 49–53
$W_u(\nu)$	PSD associated with $g_u(x)$ 46

1 Introduction

1.1 Motivation

In the last two decades, a considerable improvement in the field of wireless communication systems has been observed. This is explained not only by a continuous increase of users and Internet of Things (IoT) devices that are present in our everyday life but also by the demanding applications that each user requires [7]. Altogether, they lead to challenging requirements on the Spectral Efficiency (SE), i.e., on the effective number of bits that can be reliably transmitted over a given bandwidth. Figure 1.1 shows the continuous rising trend regarding the evolution of the number of mobile subscribers, being observed that this trend will continue in the next years. However, the available electromagnetic spectrum will remain the same, if not even more congested, which leads to challenges regarding the SE. To further complicate the system designers and network operators, wireless systems must also provide service to an increasing number IoT devices and Machine-To-Machine (M2M) as is shown in figure 1.2. Accordingly, the increase in the SE must at the same time cope with several issues, such as fading in high mobility, where multiple signal paths can disrupt the original information, user interference and path loss, i.e., the decrease in the received signal power with the distance to the transmitter. To tackle the above-stated issues, a possible solution is to consider a dense network composed of several Access Points (APs) in order to boost capacity and coverage that are necessary to meet the exponential growth of demanding users. Additionally, another solution is to employ advanced Multiple-Input Multiple-Output (MIMO) systems to increase the SE using the same bandwidth [28, 29].

Recently, traditional MIMO systems have been replaced by Massive MIMO (mMIMO) systems, which are systems composed of a huge number of antennas that form an antenna array. In Fifth Generation (5G) communications, for instance, the physical layer is supported by Base Stations (BSs) based on mMIMO systems [28, 5, 29, 18]. As a matter of fact, even though 5G technologies have been launched and deployed only recently in the majority of countries worldwide, researchers have already started to shift their focus to the next-generation wireless systems, i.e., to Sixth Generation (6G). In that sense, and

following the success of mMIMO, new antenna technologies based on Extremely Large Antenna Arrays (ELAAs) are being considered for 6G systems. Consequently, it is important to study these systems, which entails tasks such as channel modeling and channel estimation that will be the main focus of this thesis.

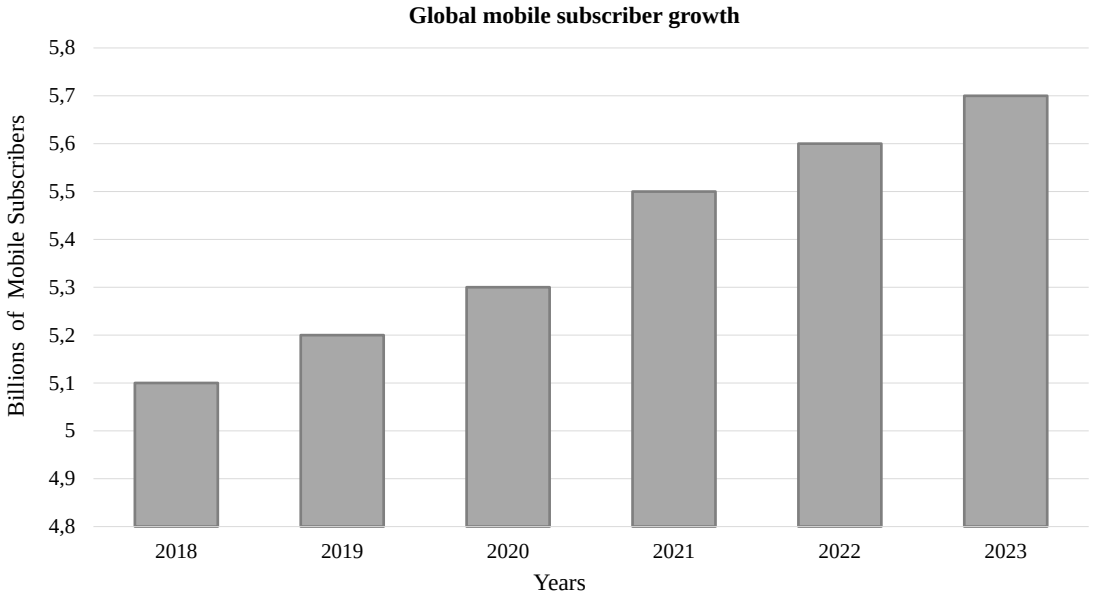

Figure 1.1: Global mobile subscriber growth - is expected to rise to 5.7 billion subscribers by 2023 from 5.1 billion users in 2018 with a 2% CAGR [7].

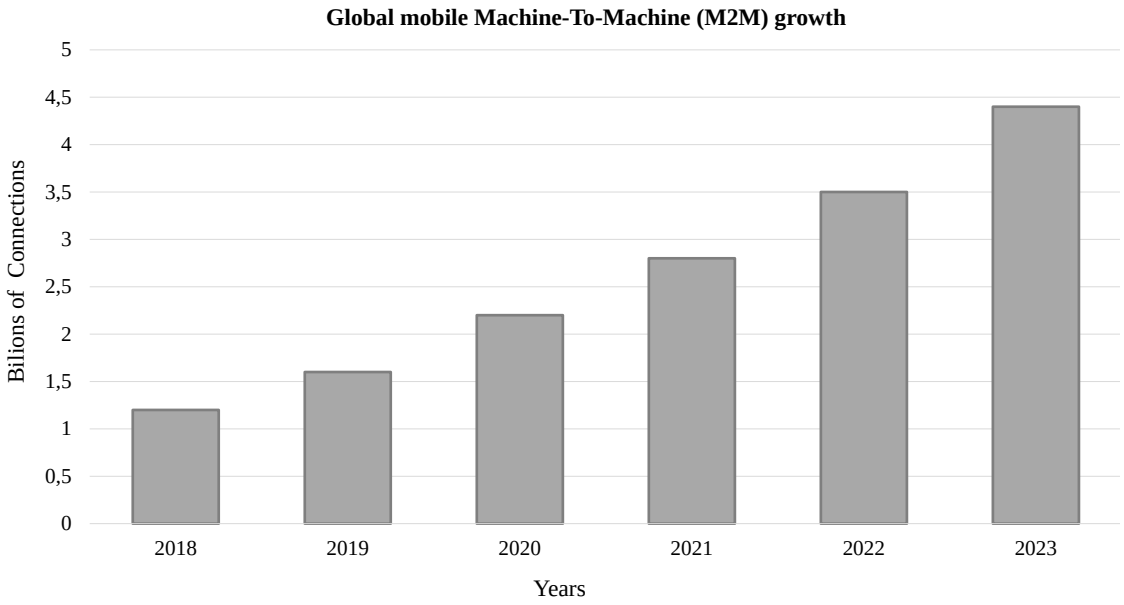

Figure 1.2: Global mobile M2M growth - its expected to rise to 4.4 billion connections by 2023 from 1.2 billion users in 2018 with a 30% CAGR [7].

1.2 Objectives and Contributions

The focus of this thesis is the channel estimation task of ELAAs. This task is crucial to enable the implementation of such systems in practical scenarios as well as to exploit their potential gains in upcoming 6G communication systems. The main results of this thesis are two low-complexity channel estimation techniques for ELAAs systems, which are summarized as follows:

- **Simulation of a Large Intelligent Surface (LIS) system and development of a low-complexity channel estimation based on spatial information**

  The first fundamental objective aims the study and analysis of spatial information to extrapolate the channels associated with the huge number of antennas of a LIS, which is used as an instance of an ELAA. For that purpose, a channel model to characterize the communication environment between the LIS system and User Equipments (UEs) was simulated in MATLAB using ray tracing. Then, it is developed a channel estimation technique that takes advantage of the spatial array geometry that considers a division of the LIS into a set of independent panels and uses information of the Angle of Arrivals (AoAs). Lastly, the performance of the channel estimation technique is accessed, and its advantages and limitations are analyzed.

- **Simulation of an Radio Stripe (RS) system and development of a low-complexity channel estimation based on spatial interpolation**

  This second main objective aims the study and development of an algorithm that uses spatial interpolation to reduce the complexity of the channel estimation task. Differently from the first goal, this algorithm is developed for a one-dimensional ELAA system, namely a RS. The RS channel model that characterizes the communication environment between the RS and UEs is implemented in MATLAB. Subsequently, it is developed a channel estimation technique that takes advantage of the spatial Fourier Transform (FT) of the channel model to aid the interpolation process. The corresponding performance results are evaluated and discussed.

1.3 Document Structure

The organization of this document and the chapters' content are presented as follows: in this introductory chapter, it is presented the problem statement of this thesis, formulating the motivation, relevance, and objectives of the analysis to be presented in the following chapters. Namely, it is briefly presented the antenna systems of the current networks and the emerging user requirements for the next generations of wireless systems, namely 6G systems.

Chapter 2 describes the state-of-the-art and further motivates the theoretical framework and methodology employed in this thesis. Firstly, mMIMO systems are explored

and analyzed in detail regarding their potential and limitations. Secondly, the current trends related to new antenna technologies for 6G are presented. In this chapter, a special focus is given to the current channel estimation techniques and their main challenges.

Chapters 3 and 4 are dedicated to the presentation of the methodology and analysis of the findings of this study regarding the design of low-complexity channel estimation techniques. Specifically, chapter 3 presents an ELAA system environment and investigates a channel estimation technique using spatial information as the array geometry and the AoA. Furthermore, the chapter 4 also presents an ELAA system environment and is dedicated to the analysis of a channel estimation technique based on spatial interpolation.

Chapter 5 concludes this thesis with a discussion regarding the problems of channel estimation in large antenna systems and the advantages and drawbacks of the proposed techniques. Lastly, some suggestions regarding possible future research directions are proposed.

2

State-of-the-Art

This chapter presents the state-of-the-art regarding the ELAAs technologies that are being envisioned for 6G communications.

Firstly, it will be discussed the actual mMIMO systems and the importance that they have by being the core antenna technology in the current 5G networks. After that, new ELAAs systems are introduced, namely LISs, RSs, and Intelligent Reflective Surfaces (IRSs). Finally, the challenges and conclusions reached by other researchers regarding these new systems will be presented, with a special focus on channel estimation issues and challenges.

2.1 Multiple-Input Multiple-Output (MIMO) Systems

MIMO systems are communication systems that have multiple Transmit (TX) and/or multiple Receive (RX) antennas that can be used to improve the throughput and link reliability, providing more Degrees of Freedom (DoF), and also to reduce interference and mitigate fading. Basically, they take advantage of the multipath propagation environments (which is usually an obstacle in single-antenna systems) to improve communications in some sense. In fact, MIMO systems can be used to serve numerous users at the same time and in the same frequency band thus fulfilling the high demand for high SE. By having multiple antennas MIMO systems yield different types of gains, such as array gains, spatial multiplexing gains and/or diversity gains [28, 29].

2.1.1 Advantages of MIMO systems

Array gain is the increase in Signal-to-Noise Ratio (SNR) achieved by the coherent and precise combining of multiple signals, either from the various TX or RX antennas that might exist in a MIMO system. Increasing the SNR boosts the range and the coverage of wireless communications.

Spatial multiplexing gain is accomplished by transmitting separate and independent signals from each different TX, enhancing the channel capacity without an increase of the utilized bandwidth. In fact, in ideal conditions, the UEs can separate the signals from

the different TX antennas, which leads to a linear increase in the channel capacity with the number of antennas of the system. Variations of this approach include transmitting the same signal in different transmit antennas, leading to diversity gains. Note that the diversity is related to the fact that the probability that at least one of the received signals does not suffer considerable fading is high, and this probability rises by increasing the number of RX antennas. These received signals can also be combined in the UE to increase the SNR.

2.1.2 Types of MIMO Systems

2.1.2.1 Point-to-Point MIMO (PP-MIMO)

MIMO systems can be classified as Point-to-Point MIMO (PP-MIMO), which is the simplest form of MIMO technology where a BS equipped with an antenna array serves a UE also equipped with an antenna array. The larger the number of antennas at the BS and/or at the UE, the greater the benefits brought by the MIMO system [23, 28, 5, 29]. The following figure 2.1 depicts the conventional architecture of a PP-MIMO system.

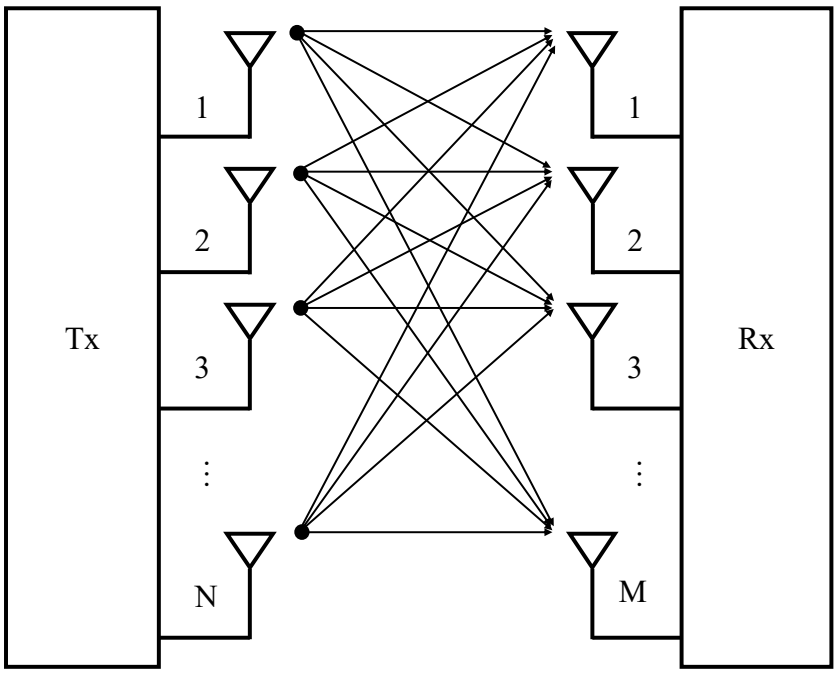

Figure 2.1: Representation of Point-to-Point MIMO system.

2.1.2.2 Multi-User MIMO (MU-MIMO)

Another type of MIMO is the Multi-user MIMO (MU-MIMO) represented in figure 2.2. It is important to consider that the main difference between these two types of MIMO is that MU-MIMO breaks the concept of the antenna array in the UE of PP-MIMO into

multiple, single-antenna UE terminals. In fact, MU-MIMO is the most used MIMO technique. This is explained by the fact that the BS has high processing capabilities and users with cellphones and/or portable computers, for example, might not be able to support a considerable number of antennas given their design and practicality.

In addition, although MIMO systems have many advantages compared to single antenna systems, they also have some drawbacks and limitations. Due to the considerably large number of antennas, the design of MU-MIMO systems becomes challenging since not only do they require low-complexity processing for channel estimation but also for separating the different data streams, as well as energy-efficient hardware such as low-resolution data converters and high energy-efficient Power Amplifiers (PAs) [29], which as a consequence might lead to performance degradation [28, 5, 29].

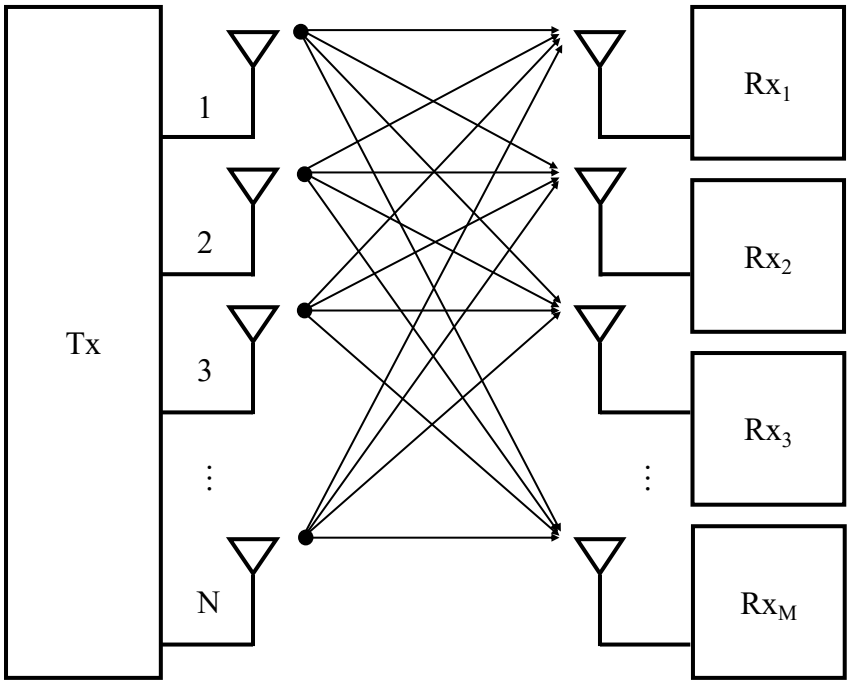

Figure 2.2: Representation of Multi-User MIMO system.

2.1.2.3 Massive MIMO (mMIMO)

The so-called mMIMO can be seen as a scaled and improved version of MU-MIMO. Furthermore, it has been a key physical-layer technology of the first 5G deployments, especially for downlink communications. It is massive not in terms of its physical size, but simply due to the fact that it involves a BS equipped with a very large number of antennas that can send and receive signals from different UEs at the same time and in the same frequency band without significant inter-user interference, which is a problem in the standard MU-MIMO systems.

With a considerably larger number of antennas, higher gains can be achieved, especially array gains, which can be used to increase the coverage of wireless communications,

or to maintain the same services using less power consumption. Having such a large BS antenna array allows more deterministic communication channels, reducing small-scale fading and frequency dependence, which might facilitate the channel estimation in UEs. This effect is referred to as channel hardening. As a result of this effect, all the signal processing operations are executed in the BSs, allowing for the reduction in hardware costs and complexity in the UEs, in contrast of MU-MIMO. All this makes mMIMO a scalable technology and justifies its adoption in 5G systems [28, 5, 29].

mMIMO takes over all the advantages of the previous MIMO technologies and reduces their drawbacks and limitations, while also bringing new improvements of its own. In the following section 2.3, a detailed analysis regarding the critical issues and major challenges of channel modeling and channel estimation techniques in mMIMO systems are presented.

2.2 Extremely Large Antenna Array (ELAA) Systems

With the deployments of MIMO and mMIMO systems it was proved that with a large number of antenna elements it is possible to improve wireless communications while serving more users. However, the number of users will continue to rise as well as the demand for better service. As stated, new communications systems need to be adaptable and improve on Quality of Service (QoS) without an inherent increase in complexity and hardware. Taking the previous arguments into consideration, new antenna technologies with ELAAs that are an extension of today's mMIMO technology are being studied and designed for the upcoming 6G.

2.2.1 Large Intelligent Surface (LIS)

LIS is a scaled-up version of the current mMIMO systems and consists of a large and thin surface integrated by a vast number of antenna elements [20]. Essentially, a LIS system can be considered as a massive dense antenna array capable of not only transmitting but also receiving radio signals in its entire surface area [14].

With densely disposed antenna elements, this conceptual ELAA system makes use of mutual coupling to accurately direct the communication channel towards the UE in the three-dimensional scope, basically enabling beamforming through an ideal Line-of-Sight (LoS) path [15, 19], as ilustrated in the following figure 2.3. For that reason, and jointly with straightforward channel estimation, it allows the increase of SNR, immense capacity gains, namely in SE, remote sensing while at the same time being capable of serving a multitude of UEs, and an accurate positioning [21].

Due to its thin flexible design and configuration, which enables a low-cost deployment and low energy consumption, LIS systems can be installed in outdoor spaces such as building facades and other likewise architectural structures [21]. However, it is important to highlight that it is more suitable for indoor communications in big industrial

and commercial spaces such as airports and shopping malls, where it can be efficiently implemented in walls and ceilings [20].

In theory, LIS can ultimately accomplish the wireless communication ambitions in the current 5G systems [15, 21] and likewise it is more adequate for today's and tomorrow's IoT applications where the need to have a high throughput and to serve a growing number of UEs, while simultaneously being able to preserve a high QoS, is expected to rise. Nevertheless, apart from the potentialities of LIS systems, there is a set of important challenges that need to be addressed.

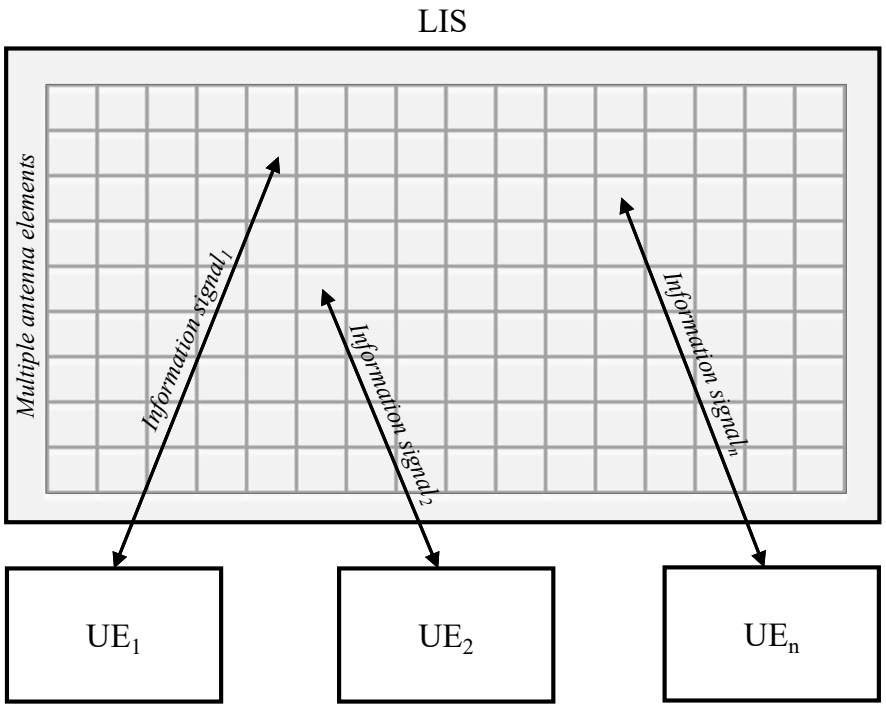

Figure 2.3: Representation of a LIS scenario with multi-user communication.

2.2.2 Cell-Free mMIMO & Radio Stripes (RS)

Cell-free mMIMO is a distributed mMIMO system that attempts to solve the inter-cell SNR limitations in cellular networks, which usually leads to large variations of the SE within the cell (i.e., the users in the cell edges might have a low spectral efficiency). In standard cell-free, there is a Central Processing Unit (CPU) which is linked to various APs through dedicated fronthaul links. The processing can be either centralized or decentralized. In the centralized processing version, the CPU makes all the processing for dealing with the uplink and downlink communications with each AP. In the decentralized version, besides having the antennas, the AP have a Signal Processing Unit (SPU) that performs some local processing [18].

A promising and cost-efficient approach to implement a cell-free mMIMO system is the RS. This system concept was created and developed by Ericsson and their prototype is represented in the following figure 2.4. In a RS system, a considerable amount of APs

are integrated into a stripe, meaning the antennas and the associated SPUs (which are called Antenna Processing Units in RS scenario depicted in figure 2.4) are serially located inside the same cable. By doing so, the need for having a dedicated backhaul between each AP and the CPU is avoided. This is made possible by using numerous antennas with very low transmit power and small low gain, resulting in reduced volume and weight with minimum heat dissipation [18, 31].

The purpose of RSs is to provide synchronization, data transfer, serial fronthaul communication, and power supply by means of a shared bus while focusing on a very discrete, effortless, and low-cost deployment of a vast number of distributed APs in the surroundings of UEs. Therefore, this system is more appropriate for densely populated areas (i.e., with a large number of UEs) where its deployment will not interfere with the surroundings and the existing infrastructure [31].

Despite their various advantages, is important to consider that RSs signals can be easily blocked since it communicates in high frequencies. Additionally, it requires precise synchronization between the SPUs and APs.

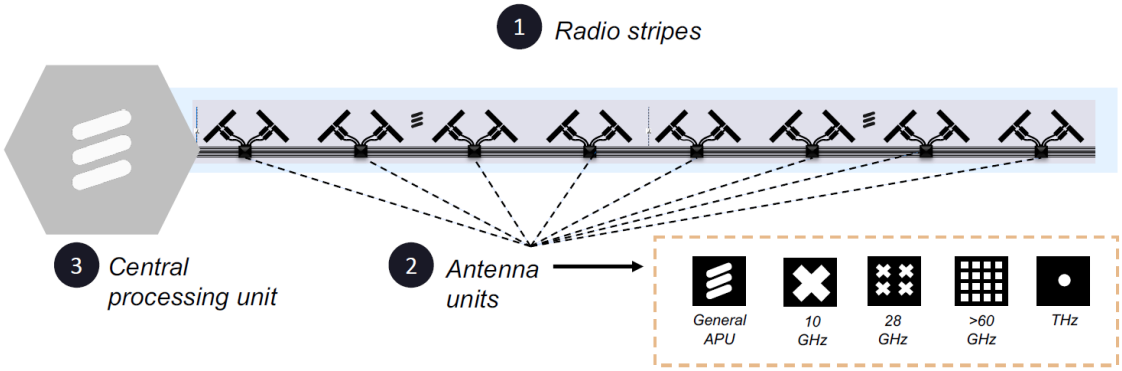

Figure 2.4: Ericsson RS prototype [11].

2.2.3 Intelligent Reflective Surface (IRS)

The IRS is a new technology concept for reconfiguring the wireless propagation environment through software-controlled reflection. The preeminent incentive to develop this technology is to overcome a major limiting factor present in current wireless communications known as fading. This last occurs due to the adverse effects that the environment has on communication performance, specifically, the uncontrollable way that physical objects and surfaces generate various propagation paths among devices through the reflection, refraction, and scattering of the transmit signal. Accordingly, these multipath components arrive at the receiver with different magnitudes, phases, and delays and can add constructively or destructively [2, 25].

IRS is a surface that encompasses numerous small, low-cost passive reflecting elements, each being separately able to control the amplitude and phase of the incident

signal. Therefore, is capable of achieving a precise reflect beamforming without the need for a dedicated energy source for signal processing, decoding, encoding, or retransmission [35, 1].

Hence, this allows us to compensate for the negative effects of multipath fading by combining the signals reflected, refracted, and scattered from other objects and/or surfaces with the desired signal or, by denying undesired multipath signals, optimizing the QoS. Additionally, IRSs can be easily implemented on buildings' facades, ceilings and walls with the scalable expense and low energy consumption.

The following figure 2.5 depicts a scenario where the LoS channel is blocked by an object and by a controlled reflection of the signal, the IRS can bypass the obstruction and deliver the signal with the intended power, leading to an improved SNR and, consequently, better QoS.

The shortcomings yet to be addressed of this new antenna concept are that it requires a significant amount of antennas in order to justify its use since it does not outperform conventional relay systems without it and the SNR is substantially inferior comparatively to mMIMO.

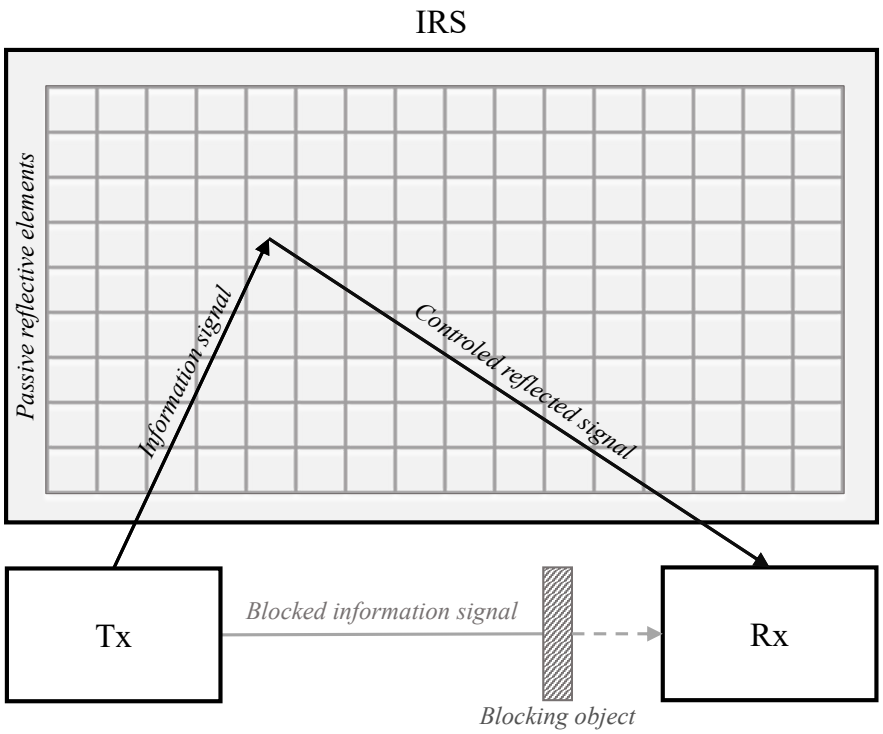

Figure 2.5: Representation of a IRS system communication.

2.3 Challenges of Communication Systems Based on ELAAs

ELAAs systems promise to achieve and deliver numerous advantages regarding current wireless communications systems. Regardless, further study is still required in order to

understand the limitations of these systems and fully exploit their main benefits.

Accordingly, the acquisition of the channel properties of a system with ELAAs in a particular deployment scenario, is an important but challenging issue. Therefore, the present section focuses on two relevant issues that have a significant impact on ELAAs systems complexity, namely channel modeling and channel estimation. In addition, different study directions by others researchers will be presented. Moreover, it is also outlined other significant concerns that should be taken into consideration regarding the ELAAs design, especially regarding LIS and RS, and compared with the current mMIMO challenges.

2.3.1 Channel Modeling

The channel model designates a mathematical equation that characterizes the wireless communication channel between the TX and RX antennas. In the time domain is the Channel Impulsive Response (CIR) and in the frequency domain is the CIR's FT, known as the Channel Frequency Response (CFR). Channel modeling is the underlying basis to test and analyze the wireless communication system performance and behavior. Channel models differ accordingly to the different communication environments and different types of systems used.

The conventional channel models for MIMO systems can have accuracy problems in LIS and RS systems. This can be explained by various reasons. One of the most prominent is the fact that such models are based on far-field approximations. However, in the new ELAAs systems, the UEs might be located in the near-field region of the serving array, which means that new appropriate channel models should be derived.

Substantiated by [27], where the authors proposed a mathematical model for communicating with a LIS that is applicable for both far-field and near-field. What separates the near-field from the far-field is the Rayleigh distance (also known as Fraunhofer distance), which is defined by

$$d_{\text{Rayleigh}} = \left(\frac{2D^2}{\lambda}\right), \tag{2.1}$$

where D is the largest dimension of the antenna array and λ represents the carrier wavelength. When the distance from the TX and RX is larger or equal to the Rayleigh distance, the spherical waves transmitted by the UE can be approximated as a uniform plane wave in the array as demonstrated in figure 2.6. With this assumption, all antenna elements in a LIS have identical signal amplitude and AoAs (i.e., face the same channel). However, if the antenna array dimension D increases, for any given wavelength λ, the UEs are more likely to be located within the Rayleigh distance and therefore in the near-field. Identifying Rayleigh distance as insufficient, the authors introduced a new distance model that complements the Rayleigh distance with the signal power and phase across array elements, since the propagation distance affects the channel both in terms of amplitude and phase. It is also referred that the variation of the aperture between antenna array

elements due to the numerous different AoAs is important, which is a characteristic commonly ignored in conventional mMIMO models, but that should be taken into account for obtaining the channel models of new ELAAs systems.

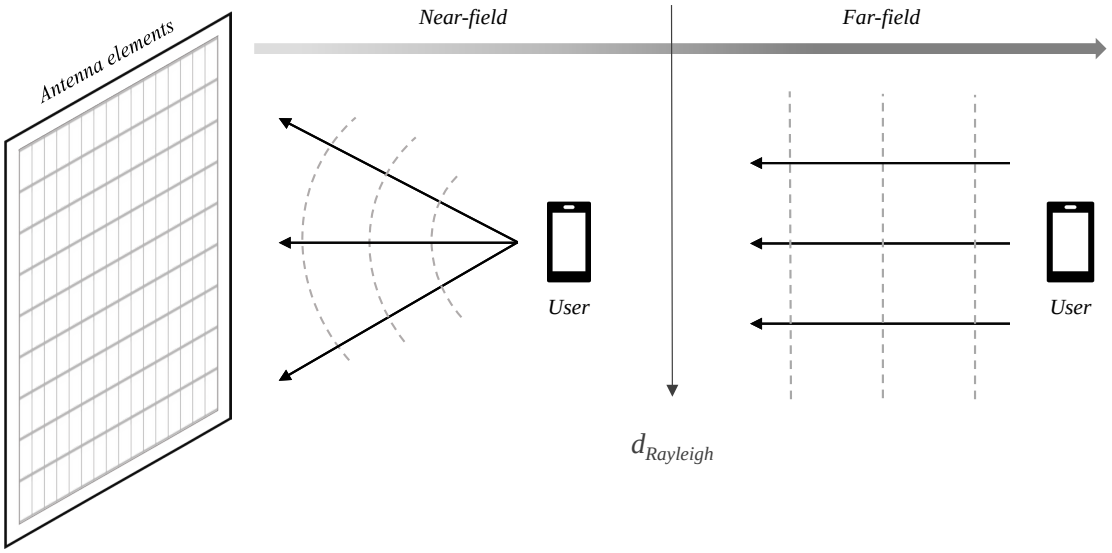

Figure 2.6: Visual representation of the differences between the near-field and the far-field regions.

In fact, the results obtained in [27] highlight the need for new channel models that are different from the conventional mMIMO models for accurate characterization of systems based on ELAAs.

Also, in [20] it is considered a near-field approximation to calculate the SE and it is compared to the far-field approximations used in conventional channel models. It is again shown that a near-field model is essential when the LIS has a comparable size to the UE distance and it becomes more prevailing as the surface enlarges. Therefore, the near-field effects should be considered when the size of the antenna system used is comparable to or larger than the distance to the UE [27, 20, 8].

The near-field effects are further laid out in [3], in which it was inferred an exact channel gain expression that encompasses these effects. In an ideal communication scenario where a single isotropic antenna with area A, perpendicular to the channel propagation direction, receives a signal from an UE at a distance d from the antenna, the received power can be calculated by

$$P_{\mathrm{rx}} = \beta_{\mathrm{d}} P_{\mathrm{tx}}, \tag{2.2}$$

where P_{tx} is the transmitted power and β_d is the channel gain. Assuming a uniform plane wave at the RX antenna, this channel gain is conventionally obtained with the following equation

$$\beta_{\mathrm{d}} = \frac{A}{4\pi d^2}. \tag{2.3}$$

This expression suggests that the channel gain can be increased by expanding the RX antenna area. However, P_{rx} can never be greater than P_{tx}, which means that the values of β_d range between 0 and 1. Additionally, N equal antennas can be implemented in an array to achieve the so-called array gain. In this scenario, the total received power can be written as

$$P_{\mathrm{rx}} = N\frac{A}{4\pi d^2}P_{\mathrm{tx}} = N\beta_{\mathrm{d}}P_{\mathrm{tx}}, \tag{2.4}$$

It is clear that the area A of the antenna array is proportional to the channel gain but the effective area depends on the UE perspective. In the previous scenario, it is assumed that all antennas are perpendicular to the channel propagation direction and, therefore, the effective area is A. However, in practical scenarios, the effective area is smaller. Therefore, the pathloss is dependent on the distance d, which varies along the array, not to mention the existence of different effective areas according to the transmission direction between the array element and the UE. In the far-field, the AoAs are similar along the antenna array, but in the near-field the discrepancy becomes more apparent and impacting. Hence, the exact expression of the total channel gain considering near-field effects and a UE centered in front of the antenna array is the following [3]

$$\alpha_{\mathrm{d,N}} = \frac{N\beta_{\mathrm{d}}}{3(N\beta_{\mathrm{d}}\pi+1)\sqrt{2N\beta_{\mathrm{d}}\pi+1}} + \frac{2}{3\pi}\arctan\left(\frac{N\beta_{\mathrm{d}}\pi}{\sqrt{2N\beta_{\mathrm{d}}\pi+1}}\right). \tag{2.5}$$

Clearly, the channel gain is not $N\beta_d$ although it is a function of it. Therefore, it can be concluded that the far-field approximation used in conventional mMIMO systems is generally accurate but ultimately, the near-field effects might have a significant impact in ELAAs systems and new channel models must be developed for enabling precise system simulations and to aid the channel estimation tasks.

There are other factors to be considered regarding a LIS system implementation, for example, channel hardening that is present in ELAA systems and therefore occurs in LIS systems as demonstrated in [21] and can simplify the equalization. Another factor is that, as higher carrier frequencies are considered, LoS communication prevails as the multipath becomes minimal [8]. In [19], the authors shift their focus to mutual coupling, which is an important aspect in ELAA systems. It is shown that mutual coupling improves the performance by accurately directing the channel to the UE with numerous densely positioned antenna elements. However, in practical deployments, reflections, scattering, and non-static environments will be a constant, and therefore more realistic models should also be considered to provide a more accurate representation of how the new ELAAs systems perform.

Nonetheless, LISs and RSs are very recent concepts and most of the channel models of the existing empirical research assume ideal environments with perfect LoS propagation and uniform plane waves by assuming far-field conditions. It is clear that the near-field conditions are important to include when channel modeling for new ELAAs systems.

In conclusion, channel modeling is very important to evaluate and improve a wireless communication system. Moreover, with an accurate channel model, new channel estimation schemes can be developed.

2.3.2 Channel Estimation

ELAAs systems are composed by a huge number of antenna elements, as the name suggests, and therefore, in order to be practically implemented, the system hardware must have low complexity and be energy efficient. Additionally, given the high number of antenna elements, it allows more and more users to communicate at the same time-frequency resource which consequently leads to large SE. Accordingly, with ELAAs systems the current processing and complexity of channel estimation techniques might be impossible to handle.

Conventional MU-MIMO represented a significant evolution in wireless communications systems, however, had some significant limitations. The most notable one is the fact that MU-MIMO is not a scalable technology. In a MU-MIMO system, in order to obtain all the gains that are capable of, the BS needs to acquire an accurate Channel State Information (CSI) of all the received signals. Therefore, CSI is very important to achieve the potential performance of the wireless communication link, due to having all the channel propagation information, allowing the system to be more adaptable to different scenarios and hence be more effective, especially in a technology with a high number of antennas. MU-MIMO was designed for systems with approximately the same number of TX and RX antennas and operates in Frequency Division Duplexing (FDD) mode. FDD, as demonstrated in figure 2.7, separates the uplink and downlink transmissions in two different communication channels with different frequencies, that is predetermined allocated, which is not ideal with an increment of UEs because it leads to a more congested bandwidth and it requires to know the CSI at both ends. To put it briefly, in a MU-MIMO system, the higher the number of antennas, the more complex and time-consuming is to accurately estimate the CSI between all the antenna elements, making this technology, not scalable [28, 5, 29].

Building on this, an improved version of MU-MIMO comes along. mMIMO has considerably larger antenna arrays and achieves improvements in spectral and energy efficiency, while being a scalable technology, diverging from the conventional MU-MIMO as a result of not operating in FDD mode. In a downlink mMIMO transmission, each BS serves a given cell and, since the channel effects are compensated at the BS, only these need to know the CSI [10, 4]. Although this can be complicated since several channels should be estimated, these systems are usually combined with Time Division Duplexing (TDD), so

that the channel reciprocity can be considered and the channel for the downlink transmissions can be estimated with uplink training [23, 10, 4, 28, 5, 29]. In TDD as exhibited in the figure 2.7, both the uplink and downlink use the same frequency channel at different time slots that can be allocated dynamically and varying in length, depending on the load requirements at the BS. Basically, the channel responses are the same in both uplink and downlink considering channel reciprocity that makes it possible to obtain accurate CSIs at the BSs that estimates the channels from pilot sequences transmitted by all the different UEs. With the help of channel hardening, previously explained in section 2.1.2.3, the generated CSIs can then be used effectively for uplink and downlink, shifting all the system complexity to the BSs. All this contributes to reducing the software and hardware level of complexity since it allows the use of simple signal processing and estimation techniques and energy-efficient components. Furthermore, the time required for channel estimation is independent of the number of BS antennas, which contributes to making mMIMO scalable and promising technology.

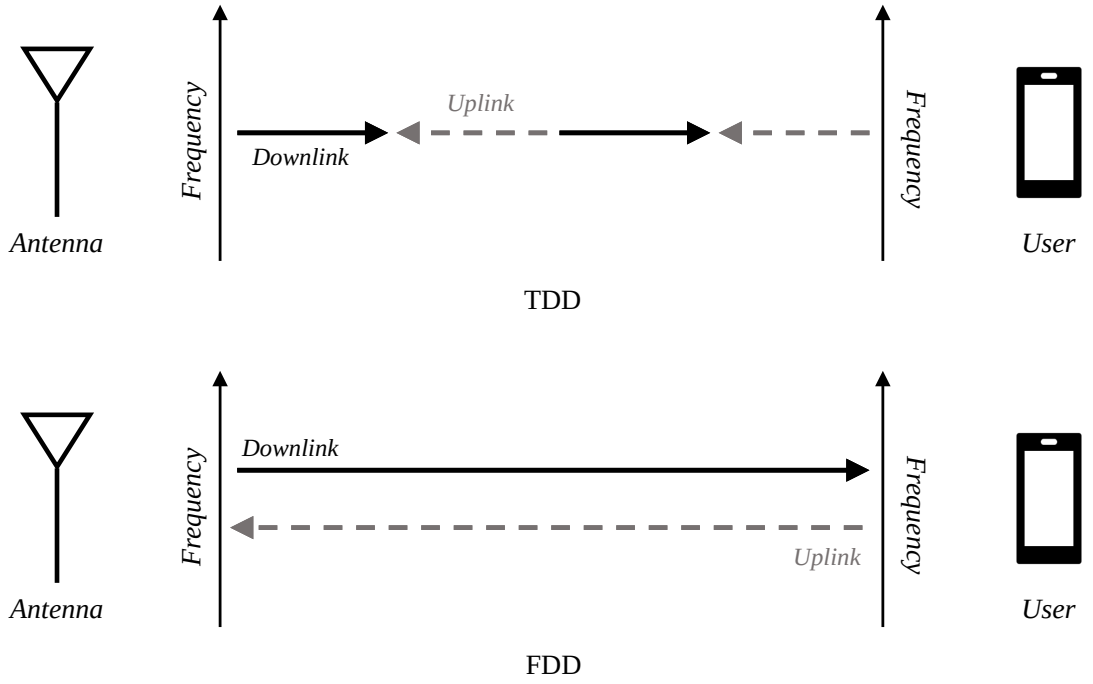

Figure 2.7: Visual representation of the TDD and FDD modes.

All the formerly presented arguments explain why mMIMO is the key technology for 5G and why the new concepts for 6G are being based on it. Despite this, mMIMO still has some limitations. One of the most notorious is an effect called pilot contamination represented in the following figure 2.8, which consists of a bottleneck regarding channel estimation. Cellular networks are constituted of various cells and due to the scarce available electromagnetic spectrum, many cells share the same time-frequency resources. As a result, it is impossible to assign different pilot sequences to all the UEs in all different

cells and so pilot sequences are repeated for different UEs. When a BS receives the pilot sequences from the UEs of a given cell, the channel estimates that come from those can be contaminated by pilot sequences of other UEs from different cells, degrading the channel estimation accuracy. It is important to note that this pilot contamination effect will persist even if the number of antennas in the BSs grows [28, 5, 29].

The goal for the 6G wireless communications is to obtain a system that can have all the advantages of mMIMO without its limitations, since the available spectrum is becoming even more congested, serving a growing number of users whilst reducing the software complexity and hardware cost. This is where the relevance of efficient channel estimation techniques is most noticeable.

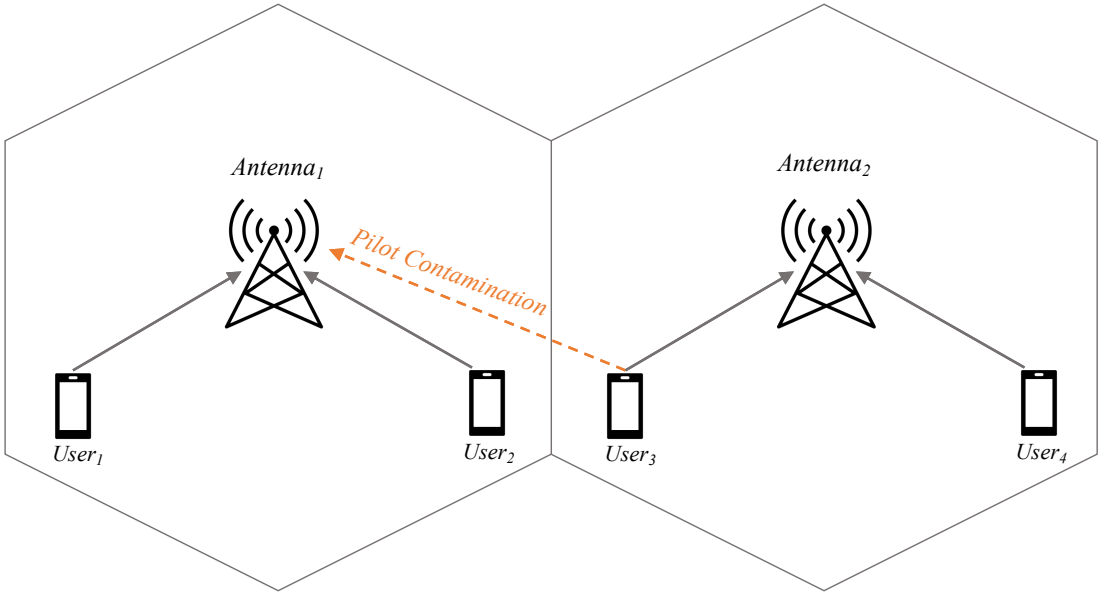

Figure 2.8: Representation of the pilot contamination effects.

According to the authors in [32], when considering a single cell scenario and taking into account a spatially correlated channel i.e., there is a correlation between the AoA of the signal and its average gain, it was drawn a comparison between Least Square (LS) estimation and Minimum Mean Squared Error (MMSE) estimation techniques for different cases, derived with the various number of antennas. Mean Squared Error (MSE) measures the average squared difference between the estimated values and the true value and accordingly allows the assessment of the channel estimation quality. LS refers to the method of regression analysis which is used to determine the best fit for a considered data set, that is minimizing the sum of the squared errors and the MMSE estimation method is a standard approach that aims to minimize the MSE. The results obtained from the research allowed the inference that MMSE estimation displayed overall better results when compared to the LS estimation technique.

It was further proven in [12] that the mMIMO systems performance is improved considerably through the adoption of an efficient channel estimator capable of delivering

robust results. This work also analyzes the performance of linear estimators such as LS and MMSE and compares them with another one developed by the authors. This last takes into consideration the fact that the true inter-cell large-scale fading coefficients are unknown due to the unreasonable effort and excessive expenses required in order to accomplish it. Hence, as a solution to this problem, the authors estimate a parameter that represents the total sum of the cross-cell large-scale coefficients plus a normalized noise variance, instead of individually estimating them as in conventional methods. The results obtained demonstrate that this proposed estimator performs in a superior manner when compared with LS estimator and is relatively close to that of the ideal MMSE estimator.

The performance degradation of the LS estimator when mMIMO system encounters pilot contamination was again discussed in [22]. This work confirms the previous statements in the literature regarding the improved results achieved in comparison with MMSE estimator and also its inherent downside of assuming perfect knowledge of cross-cell large-scale channel fading coefficients since it was previously concluded as being an unreasonable assumption. The results of this work similarly conclude that the proposed estimator delivers superior performance when compared to the LS estimator and approximate performance to the results of the ideal MMSE estimator.

It was argued and proposed in [24] that in order to minimize the channel estimation errors and improve the uplink signal-to-interference performance in mMIMO systems, the employed channel estimation technique can have a considerable impact. More specifically, it is shown both numerically and analytically that the authors' developed technique, due to inhibiting the inter-cell interference in the channel estimation, could significantly improve the system performance with the appropriate channel temporal correlation in mMIMO uplink transmission. The proposed estimator encompasses the temporal channel correlation together with the previously decoded uplink data for the current channel estimation. Taking this into account, and the fact that the estimated uplink data delivers a correspondent long pilot sequence, the results yield that it is possible to considerably repress the inter-cell interference and consequently obtain an improved channel estimation.

Therefore, it is evident from recent works of literature regarding mMIMO system that channel estimation techniques might have a considerable impact on the overall performance of the system. That being the case, channel estimation should thrive to be not only efficient but also robust and capable of delivering consistent results in most various scenarios.

With ELAAs and an exponential number of UEs, it is not practical to calculate the channel response for every single antenna element. Instead, is preferable to estimate the channel for a given number of antennas and use these estimates to estimate the remaining ones. Reducing the complexity of the channel acquisition is hence very important to reduce the overall complexity of the system and with this, numerous advantages can be obtained, such as faster communications (with low latency), low-cost hardware elements, and simplified resource allocation techniques.

2.3.3 Other Issues

There are a lot of challenges when it comes to the implementation of new wireless communication systems in general, and of ELAAs systems in particular. Even though the focus of this thesis is primarily on channel estimation, below are presented some other issues that should be taken into consideration in the system design.

One of the most notorious advantages of LIS systems performance will be the capacity to assign the available resources to different users simultaneously, however, it is not an easy goal to achieve, especially if a low level of complexity is required.

In [15], the authors proposed an optimal user allocation in a LIS system divided in smaller LIS units, considering both a LoS and a Non-Line-of-Sight (NLoS) propagation. With the intention to select the best LIS units to serve simultaneously different UEs each, it is shown, by evaluating the Received Signal Strength (RSS) at each LIS unit for each user, that near-optimal results can be achieved, contrarily to random user allocations. Moreover, following the research in [14], it is also shown that inter-user interference can be considered minimal in a LIS system, provided that far-field conditions are verified.

With a similar but more complex objective and considering a LIS divided into panels in the ceiling of a room with a perfect LoS propagation environment, the authors in [30] proposed a scenario in which the panels can either be active or not, in order to save power. According to the quality of the respective channel to the UEs, when compared to others, the panels can be activated and associated with various UEs. This is achieved using an algorithm in which the CPU communicates with the panels in order to choose the more appropriate ones, by considering optimization algorithms. Furthermore, the algorithm can turn out to be highly complex in a practical system with a large number of antenna elements and UEs. In addition, the performance results reveal that smaller panels are more efficient with more UEs communicating with the LIS, but bring higher complexity to the system.

Another important aspect to consider is the effect hardware components have on the overall system efficiency. mMIMO operates in TDD mode that makes use of channel reciprocity, which requires hardware calibration. Furthermore, Hardware Impairments (HWI) can seriously affect a communication system as is evidenced in [16], which analyzed the effect that HWI have on the performance of LIS communications for different hardware designs. It is shown that, because of HWI, increasing the size of the LIS is not always the best option as it can reduce severely the capacity of the system. Consequently, dividing the LIS into smaller LIS units, each one with a separated SPU, can mitigate the impact of HWI and facilitates deployments as well as system designs. Also, when considering low-cost hardware to implement ELAAs systems, is important to keep in mind that more impairments can be introduced, such as for instance nonlinear distortion effects.

3

Low-complexity Channel Estimation using Spatial Information

This chapter addresses and explains the methodology used to develop a low-complexity channel estimation technique for ELAAs that is based on spatial information. By recognizing that conventional channel estimation is not practical for ELAAs such as LIS, which can be composed of hundreds or thousands of antennas, the main idea of the proposed technique is to alleviate the need for estimating channels between adjacent antennas, therefore reducing the overall complexity. This is done by considering a division of the LIS into a set of panels and also using AoA information. In the following sections, this technique is described for a baseline communication scenario that consists of an uplink communication between a LIS and UEs in an indoor room.

3.1 System Characterization & Channel Modeling

The proposed technique is based on a channel model that characterizes the propagation environment between the LIS and UEs in an indoor room and assumes the plane-wave regime (i.e., the communication occurs in the far-field region). In the considered communication environment, the LIS is a flat surface, with a square format (i.e., the same number of antennas per dimension), centered on the ceiling of an indoor room with specific dimensions, as can be seen in figure 3.1. Furthermore, it is assumed that the LIS system is operating with frequency f_c and thus, i.e., wavelength $\lambda = c/f_c$, with c representing the propagation speed of light in vacuum. Moreover, in the considered baseline uplink scenario, it is assumed that the LIS can serve up to U users, each one transmitting with unitary power, i.e., $P_{tx} = 1$ W.

Channel modeling is fundamental for evaluating the performance of wireless communication systems. This is explained by the fact that channel models can be used for performing extensive simulations and perform stress tests, allowing the system design to be more robust prior to the implementation phase. In this section, the basics of the propagation of the considered communication scenario as well as the considered channel model used to derive CIR and the CFR are presented.

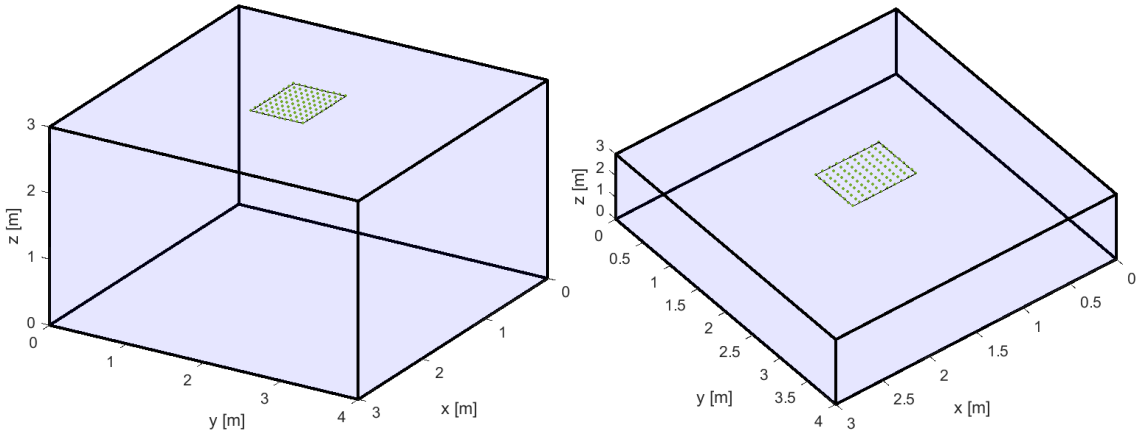

Figure 3.1: Representation of the LIS (in green) in the ceiling of an indoor room from two different viewing angles.

Let us start by assuming that the UEs and the LIS communicate in the far-field region and both have isotropic antennas (antennas that radiate equally in all directions with the same intensity). Unless otherwise stated, it is considered that the position of the UEs inside the room is randomly generated.

The considered channel model is a geometric channel model supported by geometric optics, namely first-order reflection ray-tracing techniques [34]. Geometric optics is a widely used concept in optics, where rays are defined as geometric straight lines which originate from their source (in this case, UE) and travel through the environment (i.e. ray paths). The room is considered free of obstacles (for all intents and purposes, the location of the LIS in the ceiling is useful to support the adoption of this assumption). With these assumptions, there are a total of $I = 5$ rays per UE in the empty room, more concretely one for the LoS component (identified with index $i = 1$) and the remaining accounting for the reflections associated with the four walls (which are numbered from $i = 2$ to $i = 5$). Figure 3.2 shows the scattering communication environment in the room when one user ($U = 1$) is communicating with the LIS. The users' images are represented so that the scattering environment can be better depicted.

Ray tracing is a method for estimating the propagation links between a given transmit-receive antenna pair. Therefore, it can be used to estimate the corresponding wireless communication channels, allowing the calculation of the pathloss, AoA, and propagation delay of the different signal paths arriving at the receiver.

The ray tracing method provides a visual tool that facilitates the understanding of different propagation mechanisms. By being combined with a plane wave approximation, it allows the signal paths in the indoor room to be seen as narrow beams, which are designated as rays [36, 6]. The main goal is to identify the power and the delay of the different rays in such a manner that the CIR can be derived and a channel model is generated.

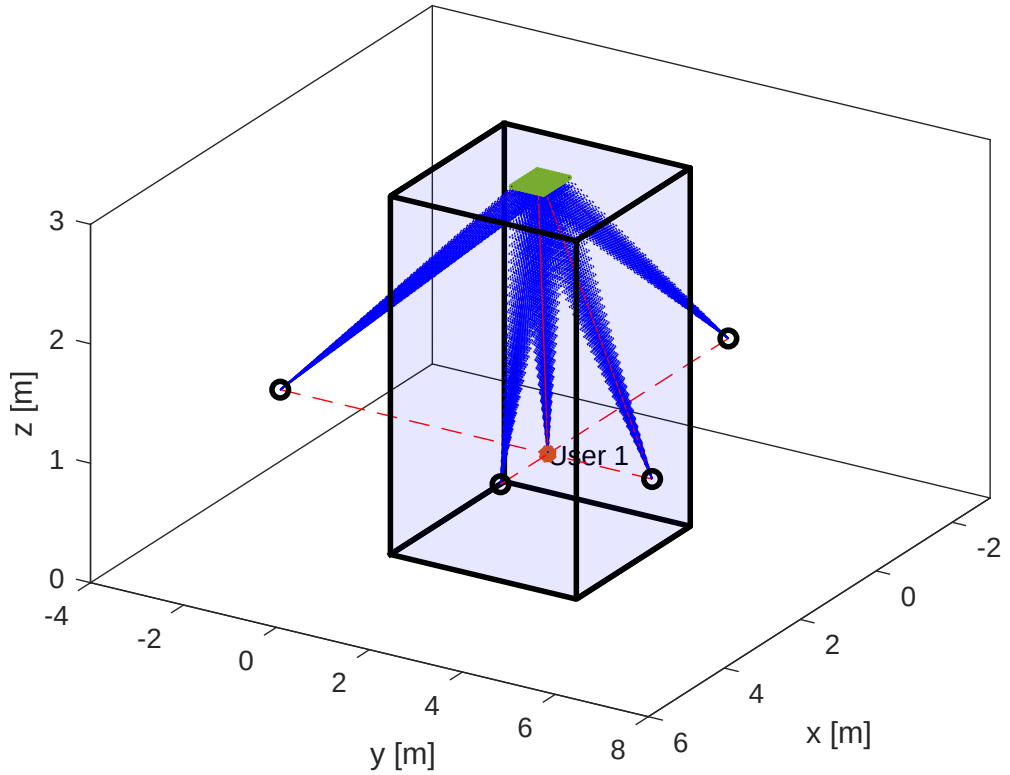

Figure 3.2: Representation of the scattering communication environment between one user and the LIS (in green) in an indoor room.

As previously stated, there are a total of $I = 5$ rays per user. Namely, one LoS component and four reflected rays that correspond respectively to the four walls of the indoor room, since only the first-order reflected rays are being considered. For the purpose of obtaining the powers and delays of the I rays of each one of the antenna elements, the distance propagated by each ray needs to be calculated. The ray tracing method and more concretely the images method (also known as images technique) considered for deriving the channel model of the uplink LIS scenario is represented in figure 3.3. As can be observed from the figure, the images method can determine the trajectory of the ith reflected ray between the user u and the receive antenna r. The images method is explained as follows:

- Firstly, it is located the image of the uth user (i.e. the mirror image with respect to a symmetry hyperplane), denoted as u', with reference to the reflection surface in the indoor room, which in the considered environment can be one of the four walls;
- Then, it is made a connection between r and u' in order to derive a line that intersects the reflection surface;
- Finally, the propagation distance of the ith reflected ray is the length of this line.

Therefore, in the considered propagation environment, the ith ray associated with the uth user travels a distance $d^{(r,u,i)}$ to the antenna r. This distance can be calculated as

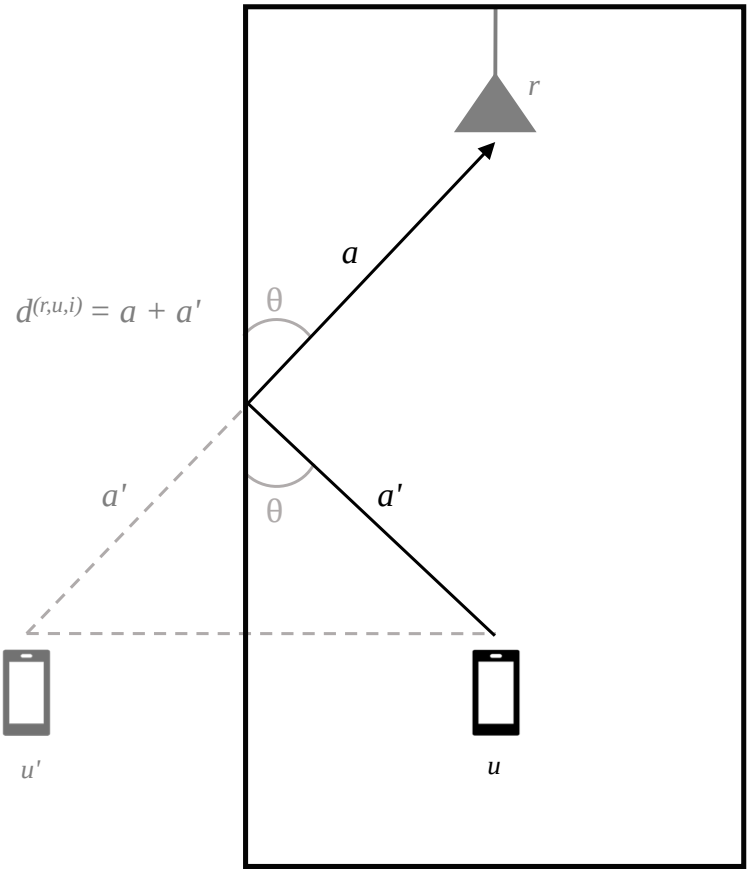

Figure 3.3: Illustrative representation of the images method used for ray tracing.

follows

$$d^{(r,u,i)} = \sqrt{(x_r - x_u)^2 + (y_r - y_u)^2 + (z_r - z_u)^2}, \tag{3.1}$$

where (x_r, y_r, z_r) and (x_u, y_u, z_u) are the three-dimensional coordinates of the rth antenna of the LIS and of the uth user, respectively. Note that this equation also applies to the reflected rays' distance, meaning that $d^{(r,u',i)} = d^{(r,u,i)} = a + a'$, where a and a' are the distances represented in figure 3.3. Using the complex baseband representation of a Linear Time-Invariant (LTI) channel, the complex amplitude of a given ray can be written as

$$\bar{\alpha}^{(r,u,i)} = |\bar{\alpha}^{(r,u,i)}| \exp\left(-j\frac{2\pi d^{(r,u,i)}}{\lambda}\right). \tag{3.2}$$

In fact, both the phase and magnitude of the complex-valued ray can be computed with the knowledge of the propagation distance. When illuminated by the ith ray associated with the uth user, the antenna r captures an amount of power that can be estimated by Friis' formulas [13]. By assuming isotropic TX and RX antennas, the received power associated with a given ray is

$$P_{rx}{}^{(r,u,i)} = \left(\frac{\lambda}{4\pi d^{(r,u,i)}}\right)^2 P_{tx}, \tag{3.3}$$

where P_{tx} is the transmitted power. Under these conditions, the magnitude of the complex ray (r,u,i) is

$$|\bar{\alpha}^{(r,u,i)}| = \sqrt{P_{rx}{}^{(r,u,i)}}. \tag{3.4}$$

Moreover, having in mind that the phase of the reflected rays can be changed by the reflection coefficient of the corresponding reflective surface, we can write the complex amplitude associated with the ray (r,u,i) as

$$\bar{\alpha}^{(r,u,i)} = \begin{cases} \sqrt{P_{rx}{}^{(r,u,i)}} \exp\left(-j\frac{2\pi d^{(r,u,i)}}{\lambda}\right) & \text{if } i = 1 \\ \sqrt{P_{rx}{}^{(r,u,i)}} \exp\left(-j\frac{2\pi d^{(r,u,i)}}{\lambda}\right) \Gamma_i & \text{if } i > 1, \end{cases} \tag{3.5}$$

where Γ_i is the reflection coefficient associated to the ith wall reflection. Each ray can be normalized to guarantee unitary average channel gains. Moreover, it was considered the possibility to have an additional fading component $\beta_i \sim \mathcal{CN}(0,1)$ in each ray in order to have a more realistic representation of the propagation channel, so that

$$\alpha^{(r,u,i)} = \begin{cases} \dfrac{\bar{\alpha}^{(r,u,i)}}{\sum_{i=0}^{I-1} \bar{\alpha}^{(r,u,i)}} \beta_i & \text{if } i = 1 \\ \dfrac{\bar{\alpha}^{(r,u,i)}}{\sum_{i=0}^{I-1} \bar{\alpha}^{(r,u,i)}} \beta_i \Gamma_i & \text{if } i > 1. \end{cases} \tag{3.6}$$

The delay associated with the ray (r,u,i), i.e., the time that takes a signal to reach its destination can be easily computed by knowing the propagation distance and the speed of light, namely

$$\tau^{(r,u,i)} = \frac{d^{(r,u,i)}}{c}. \tag{3.7}$$

By having the complex amplitude and the delays of each ray, one can obtain the CIR between the rth antenna and the uth user by using the following equation

$$h(t)^{(r,u)} = \sum_{i=1}^{I} \alpha^{(r,u,i)} \delta\left(t - \tau^{(r,u,i)}\right). \tag{3.8}$$

Consequently, the CFR is the Fourier transform of $h(t)$, i.e.,

$$H(f)^{(r,u)} = \sum_{i=1}^{I} \alpha^{(r,u,i)} \exp(-j2\pi f \tau^{(r,u,i)}). \tag{3.9}$$

3.2 Low-complexity Channel Estimation Algorithm based on the Angles of Arrival (AoA)

As previously stated, a LIS system is composed of a huge number of antennas, making impractical and time-consuming the use of the conventional channel estimation techniques based on the transmission of orthogonal pilots sequences [28, 5, 29]. Therefore, simplified channel estimation techniques must be developed so that the benefits of using ELAAs can be fully exploited. The main idea of the proposed algorithm is to consider a division of the LIS surface into panels and investigate whether the use of one pilot per panel is enough to obtain a small estimation error in the channel of all antennas of the panel. Therefore, the number of panels is not fixed and can change. The interpolation of the channels of antennas in the panel that doesn't have a pilot associated is made using AoAs information.

A considerable number of studies, evaluations, and research projects regarding the AoA estimation in antenna arrays have been conducted over the years. In [17], the researchers used a multiple signal classification algorithm to estimate the AoAs for a MIMO system with uniformly-spaced one-dimensional array antennas. This algorithm requires a data matrix composed of the received baseband waveforms and an estimated correlation matrix. The spectrum's peaks correspond to the AoA of the signals. It was proven that a multiple signal classification algorithm improves significantly the AoA estimation. This improvement is better for better correlation matrices. As an evolution of [17], the study in [9] also highlights the usage of a multiple signal classification algorithm in order to estimate the AoA with regard to a mMIMO system.

Moreover, [33] reports that the estimated AoAs of a two-dimensional antenna array are acquired through a low complexity algorithm, which refers to a unitary estimation of signal parameters via rotational invariance techniques. This algorithm uses information about the antenna array, namely the spacing between antenna elements and the array size, and signal information such as wavelength. The study findings were shown to be positive and it was concluded that the results depend on the antenna array configuration, i.e., whether the azimuth estimation or the elevation estimation is more valued, is better to have an array with more antennas in the x axis or the y axis correspondingly (the azimuth angle and the elevation angle will be explained further in this section). For an improved overall AoA estimation, a balanced configuration is recommendable.

None of this research use information about the UE that communicates with the antenna array. However, in this thesis, the method considered takes into account that the user position is accurately known inside the indoor room.

Let us consider that the LIS has a square format (i.e., the same number of antennas per dimension) as previously highlighted. However, let us now assume that the LIS is composed of P panels also with a square format. Each panel is composed of $a_p = {a_{ps}}^2$ antenna elements, where a_{ps} is the number of antenna elements per each side of the panel. Therefore, the LIS has a total of $M = P \times a_p$ receive antennas. Accordingly, the representation of the LIS is shown in the following figure 3.4.

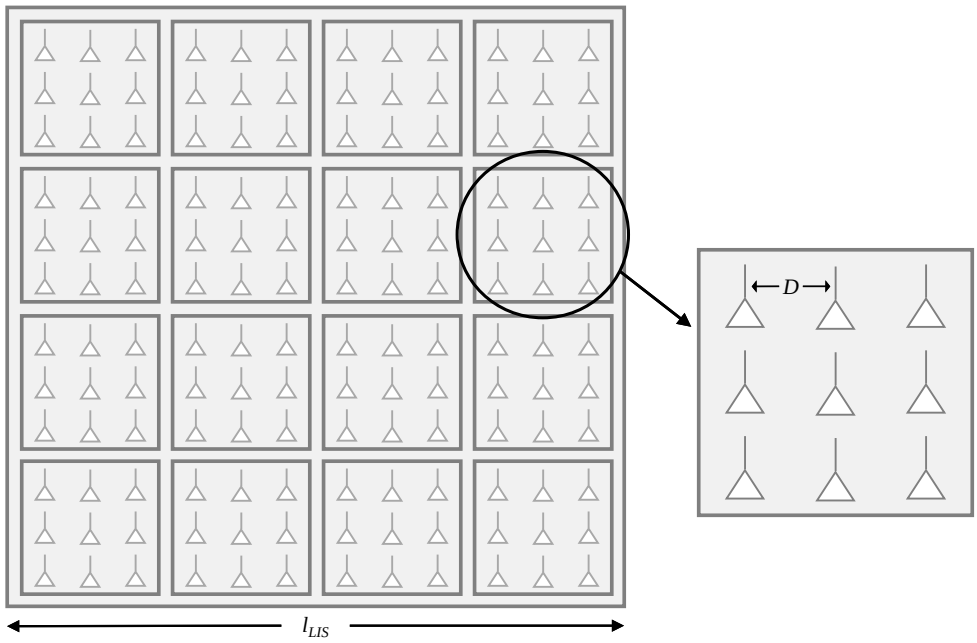

Figure 3.4: Representation of the LIS divided into panels and the respective antenna elements of each panel.

The distance between antenna elements a_p is defined by $D = \lambda/2$. The length of the side of the LIS is given by $l_{LIS} = (\sqrt{M} - 1) \times D$ and, since it has a square format, the LIS's area is accordingly calculated by $A_{LIS} = {l_{LIS}}^2$.

Please note that the reference antenna of a panel p and for which the channel is estimated (for instance with conventional uplink pilots) is considered to be the antenna located in the first position of the array and is the one used as a reference for the remaining antennas. For example, if the number of panels is $P = 1$, meaning that the LIS is being considered in its entirety as one panel, its going to be only used 1 pilot (associated with the reference antenna) to estimate all the other antennas' channel in the LIS. On another hand, if the number of panels is $P = 16$, its going to be used 16 pilots, one per each reference antenna of each correspondent panel p.

Table 3.1 displays and summarizes the important information regarding the characteristics of the uplink LIS communication system used throughout the analysis of this technique.

Parameter	Description
f_c	Carrier frequency
$\lambda = c/f_c$	Wavelength
$D{=}\lambda/2$	Spacing between antenna elements
P	Number of panels (has the format $P = 4^n$)
a_{ps}	Number of antennas per each panel side
$a_p = {a_{ps}}^2$	Total number of antennas per panel
$M = P \times a_p$	Total number of antennas in the LIS
$l_{LIS} = (\sqrt{M} - 1) \times D$	Length of the LIS side
$A_{LIS} = {l_{LIS}}^2$	Area of the LIS
A_{ir}	Area of the indoor room
U	Number of users
$P_{tx} = 1$	Transmit power
I	Rays (i.e., multipath components) per user

Table 3.1: Parameters associated with the design of the LIS and the communication environment.

The AoAs of the reference antenna, namely, the azimuth angle (denoted by $\varphi_{ref}^{(p,u,i)}$) and the elevation angle (denoted by $\theta_{ref}^{(p,u,i)}$), which are represented illustratively in figure 3.5, are calculated by the following respective equations

$$\varphi_{ref}^{(p,u,i)} = \arctan\left(\frac{y_u - y_{ref,p}}{x_u - x_{ref,p}}\right), \tag{3.10}$$

and

$$\theta_{ref}^{(p,u,i)} = \arccos\left(\frac{z_{ref,p} - z_u}{d^{(p,u,i)}}\right), \tag{3.11}$$

where x_u, y_u, z_u are the coordinates of a uth user, $x_{ref,p}, y_{ref,p}, z_{ref,p}$ are the coordinates of the pth reference antenna and $d^{(p,u,i)}$ is the distance the ith ray associated with the uth user travels to the pth reference antenna (which can calculated as shown in equation (3.1)). By using this model, the main goal is to estimate the channel in one antenna of pth panel and extrapolate the remaining channels of that panel using only the information about the AoAs.

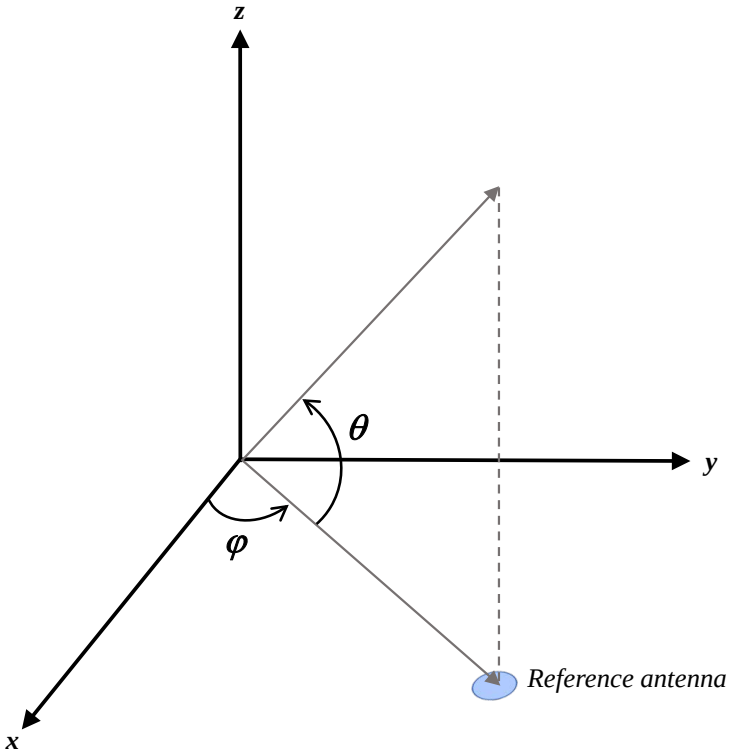

Figure 3.5: Illustrative representation of the AoA - azimuth (φ_{ref}) and elevation (θ_{ref}).

After calculating the azimuth and elevation angles of the chosen reference antenna of a given panel p, which in the proposed system is always the first antenna of the antenna panel, it is then extrapolated the information required for the determination of the CIR of the remaining antennas. Firstly, it was estimated the difference in the propagation distance between the user and the remaining antennas of the panel by converting the spherical coordinates ($\varphi_{ref}^{(p,u,i)}$ and $\theta_{ref}^{(p,u,i)}$) to rectangular coordinates as follows

$$\begin{aligned}\Delta_d^{(p,r,u,i)} = &\left(d_y^{(p,r)} \times D \times \sin\left(\theta_{ref}^{(p,u,i)}\right) \times \sin\left(\varphi_{ref}^{(p,u,i)}\right)\right) \\ &+ \left(d_x^{(p,r)} \times D \times \sin\left(\theta_{ref}^{(p,u,i)}\right) \times \cos\left(\varphi_{ref}^{(p,u,i)}\right)\right),\end{aligned} \tag{3.12}$$

where D is the distance between antenna elements, as represented in table 3.1. The variables $d_x^{(p,r)}$ and $d_y^{(p,r)}$ are integers that represent the relative distance between the reference antenna and the antenna that is being estimated. As illustrated in the following figure 3.6, the reference antenna (in blue), considered as the first antenna of the antenna array that constitutes each panel p, is on the relative position (1,1) on the two-dimensional coordinate plane. Additionally, an antenna that is positioned on (2,3) in the antenna array, which means that it is separated by D in the x axis and by $2\times D$ in the y axis thus, $d_x^{(p,r)} = 1$ and $d_y^{(p,r)} = 2$.

After $\Delta_d^{(p,r,u,i)}$ is determined in the previous equation (3.12), the phase difference can also be estimated by the following equation

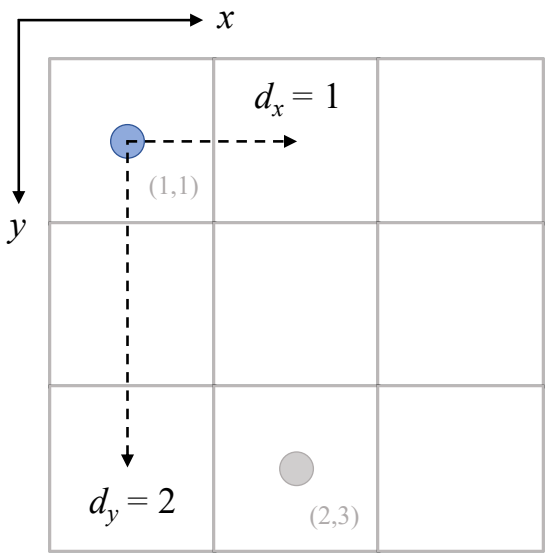

Figure 3.6: Illustration of variables d_x and d_y that represent the relative distance between the reference antenna and another antenna of a given panel.

$$\Delta_{\varphi}^{(p,r,u,i)} = \varphi_{ref}^{(p,u,i)} + \frac{2\pi\ \Delta_{d}^{(p,r,u,i)}}{\lambda}. \tag{3.13}$$

Finally, the complex amplitude of the ith ray of the communication link between the uth user and the rth receive antenna is

$$\hat{\alpha}^{(p,r,u,i)} = \sqrt{P_{ref}^{(p,u,i)}} \times \exp(j\Delta_{\varphi}^{(p,r,u,i)}), \tag{3.14}$$

where $P_{ref}^{(p,u,i)}$ is the power of the reference antenna which is calculated by the previous equation (3.3).

For the purpose of evaluating the efficiency of the proposed extrapolation technique, we define the Normalized Mean Squared Error (NMSE) of the channel estimates, so that the estimation error can be measured. The NMSE is computed as follows

$$NMSE = \frac{\sum_{i=1}^{I} \left| \alpha^{(r,u,i)} - \hat{\alpha}^{(p,r,u,i)} \right|^2}{\sum_{i=1}^{I} \left| \alpha^{(r,u,i)} \right|^2}, \tag{3.15}$$

where $\alpha^{(r,u,i)}$ is the true ray defined in equation (3.6) and $\hat{\alpha}^{(p,r,u,i)}$ is its estimated version obtained through the extrapolation process described above. In the next section, a set of performance of this estimation process results are shown.

3.3 Performance Results

In this section, it is provided the obtained simulation results that enable the analysis of the channel estimation performance, which is evaluated considering different possible scenarios. In addition, it should be noted that the simulation experiment was implemented in accordance with the methodology in sections 3.1 and 3.2.

In the simulations and for all the conceptualized scenarios, the parameters concerning the carrier frequency $f_c = 2$ GHz, which results in the wavelength being $\lambda = 0.15$ m $= 15$ cm and consequently the distance between antenna elements $D = 7.5$ cm are considered constant. In addition, unless stated otherwise, it is also considered unchanged the following parameters that characterize the LIS design: the number of panels $P = 1$, meaning that the LIS is being considered in its entirety as one panel, and the total number of antennas per panel $a_p = 100$. That being the case, the total number of antennas in the LIS is accordingly $M = 100$. Additionally, it is considered that the area of the indoor room is $A_{ir} = 12$ m^2, where the x axis has a length of 3 m and the y axis of 4 m.

It should also be noted that for all the following figures presented, the reference antenna of a panel p is identified by red rays or is marked with a red circle. This antenna is where the channel is estimated (for instance with conventional uplink pilots) and is the one used as a reference for estimating by extrapolation the channel of the others.

Starting with the scenario depicted in figure 3.7, the LIS is at a $z = 3$ m and it communicates with two users ($User$ 1 and $User$ 2).

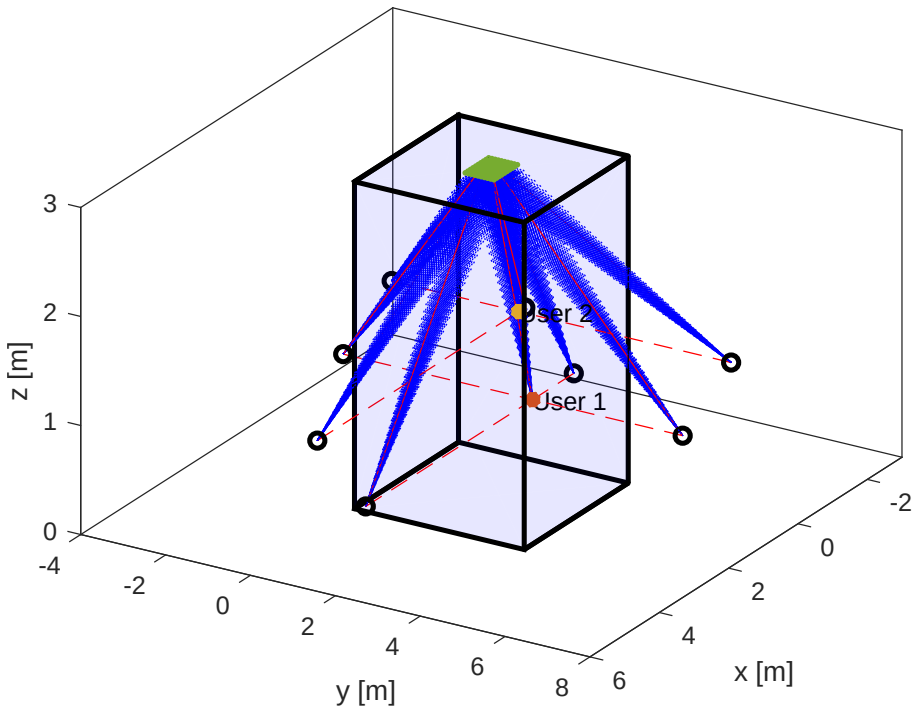

Figure 3.7: Indoor room scattering communication scenario with two users ($User$ 1 and $User$ 2) with randomly generated positions and the LIS at $z = 3$ m.

Additionally, the users' positions in the indoor room are randomly generated.

Fig. 3.8 below shows the NMSE the measurements for each antenna in a LIS regarding the scenario depicted in figure 3.7.

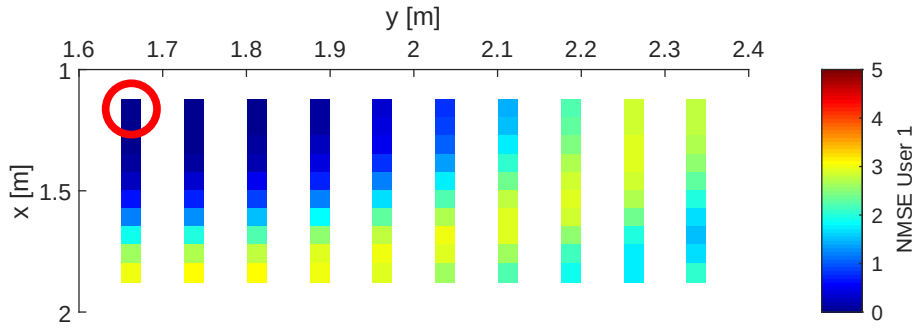

(a) NMSE measurements for User 1.

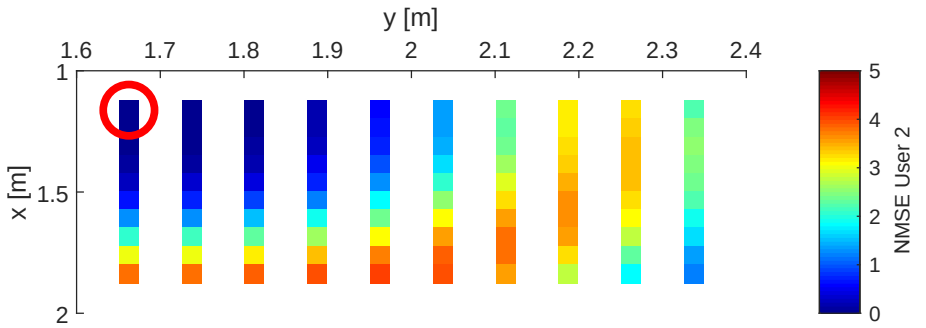

(b) NMSE measurements for User 2.

Figure 3.8: NMSE measurements for each antenna in a LIS regarding the scenario depicted in figure 3.7.

From the figure, it can be observed that the NMSE is close to zero in the antennas near the reference antenna and it gets worse as the distance to the reference antenna increases. It is also observed that the NMSE depends on the position of the user, i.e., has better results if the user is far away from the LIS, in this case, *User* 1. This behavior is expected considering that, as the user is getting farther away from the LIS, the calculated distance difference using the AoAs will become increasingly precise.

3.3.1 Line-of-Sight (LoS) Communication Environment

Further demonstrating this effect, let us consider a different scenario in which the ceiling of the indoor room, where the LIS is situated, has now 10 meters of height, i.e., $z = 10$ m, and communicates only through LoS propagation with a user at $z = 1$ m centered with the panel, as represented in figure 3.9.

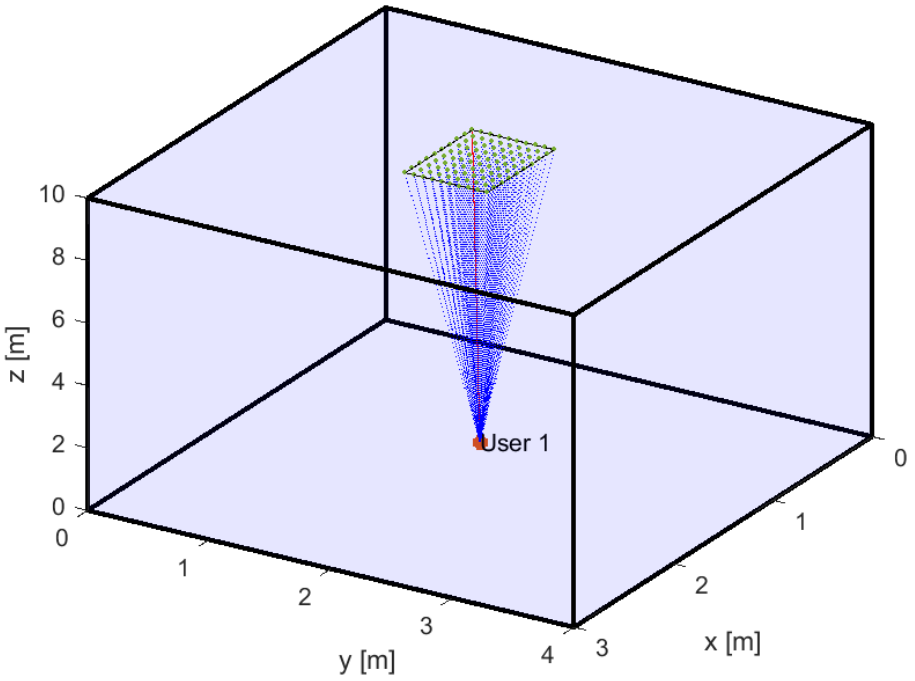

Figure 3.9: Indoor room LoS communication scenario with one user at $z = 1$ m centered with the LIS, which is at $z = 10$ m.

Figure 3.10 presents the NMSE of the channel estimate considering the scenario of figure 3.9. As it can be noticed from the figure, the NMSE exhibits favorable results for most of the antenna elements that compose the LIS. As previously stated, this effect can be explained due to the fact that the parallel rays approximation behind the extrapolation process is tight, thus increasing the accuracy of the channel model based on the AoAs.

In contrast, note that when the user moves to a position closer to the LIS, worse estimation results are expected. Figure 3.11 presents the NMSE when the user is at $z = 9$ m.

The lower estimation performance can be explained due to the fact that the phase approximation for the different channels of the LIS is not being well estimated using the parallel rays approximation. Therefore, the accuracy of this channel estimation process based on the AoAs is clearly dependent on the relative distance between the user and the antenna array.

Considering results from figures 3.10 and 3.11, it can be concluded that the channel estimation complexity can be reduced since it might not be required to obtain the CIR for all antennas in a LIS.

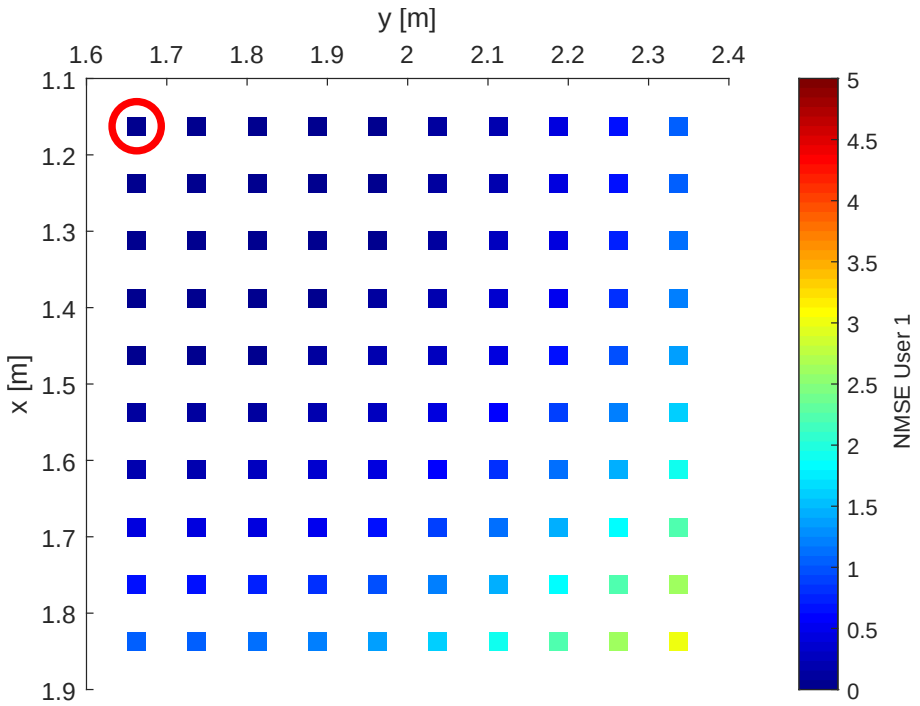

Figure 3.10: NMSE measurements for each antenna in a LIS regarding the scenario depicted in figure 3.9.

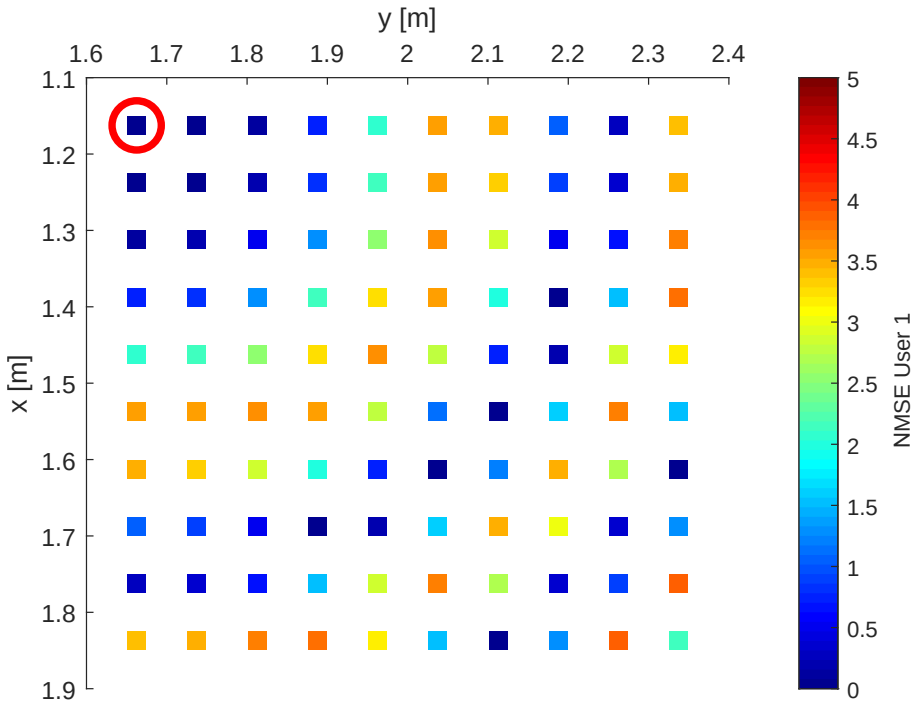

Figure 3.11: NMSE measurements for each antenna in a LIS regarding the scenario depicted in figure 3.9 except now with the user at $z = 9$ m.

So far, only antenna arrays (i.e., LIS) with $M = 100$ antennas in a single-panel fashion were considered. In order to accurately evaluate the effect that the total number of antennas has on the channel estimation complexity, let us consider a more realistic scenario in which the LIS is placed on a ceiling with height $z = 3$ m and communicates with one user that is centered with the panel at $z = 1$ m, portrayed in 3.12.

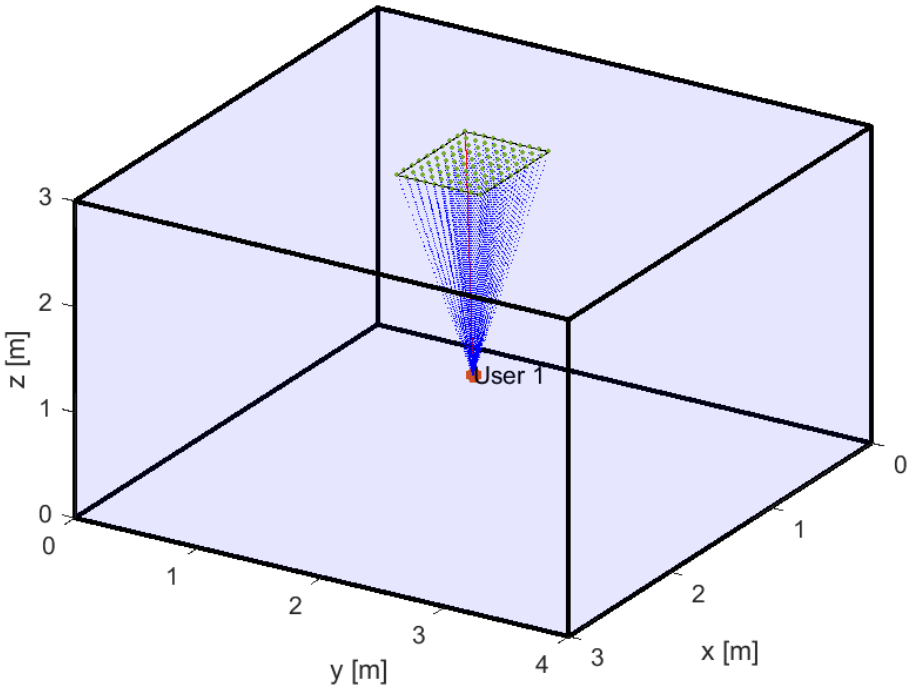

Figure 3.12: Indoor room LoS communication scenario with one user at $z = 1$ m centered with the LIS, which is at $z = 3$ m.

For a LIS with a total of $M = 100$ in a single-panel design, the results of the channel estimation technique of the considered estimation process can be seen in figure 3.13 for $M = 100$ and in when the LIS is comprised of $M = 400$ antennas in figure 3.14.

From the figures, it is possible to observe that the number of antennas for which the channel estimation is not favorable is higher since the LIS has only a single panel and there is one reference antenna to extrapolate the remaining channels. Hence, when the number of panels is increased and therefore a higher number of reference antennas (one per panel) are available, the channel estimation improves significantly. Maintaining the same total number of antennas $M = 400$ and distributing in $P = 4$ panels, each with $a_p = 100$ antennas, some improvements can be noticed as shown in figure 3.15.

These findings continue to be observed for larger values of P, which is expected since the number of reference antennas also increases. For example, when considering again $M = 400$ and dividing the LIS into by $P = 16$ panels, each with $a_p = 25$ antennas as exemplified in figure 3.16 (which means that its going to be used only 16 pilots, one per each reference antenna). Figure 3.17 shows the achievable NMSE considering the LIS design of figure 3.16.

The results confirm the previous conclusions, i.e., for LIS with a large number of

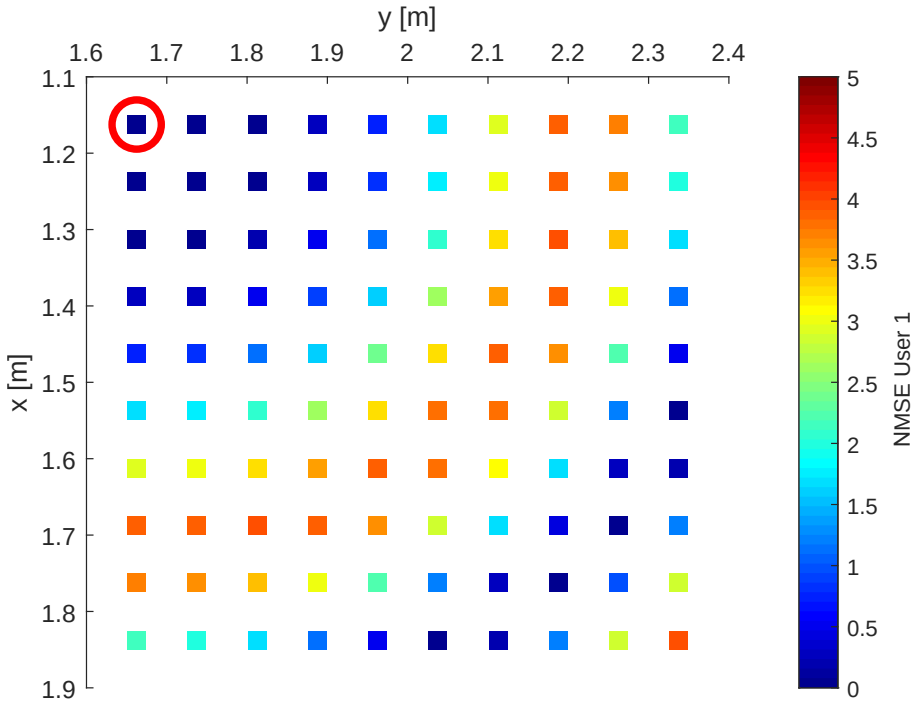

Figure 3.13: NMSE measurements for each antenna in a LIS, considering only a LoS communication scenario with one user at $z = 1$ m, centered with the LIS positioned at $z = 3$ m and with $M = 100$ total antennas.

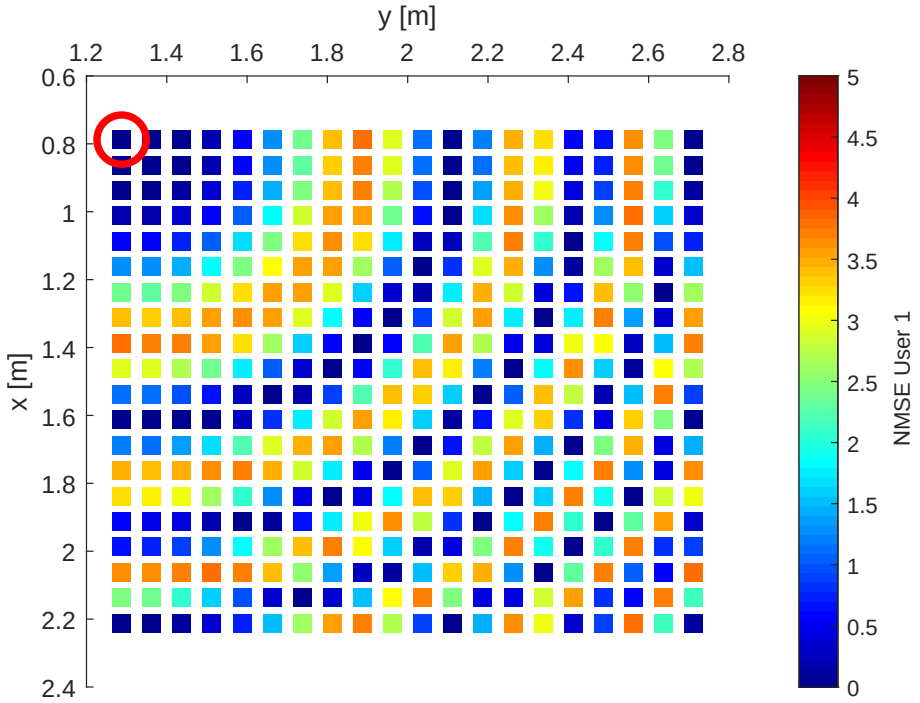

Figure 3.14: NMSE measurements for each antenna in a LIS, considering only a LoS communication scenario with one user at $z = 1$ m, centered with the LIS positioned at $z = 3$ m and with $M = 400$ total antennas.

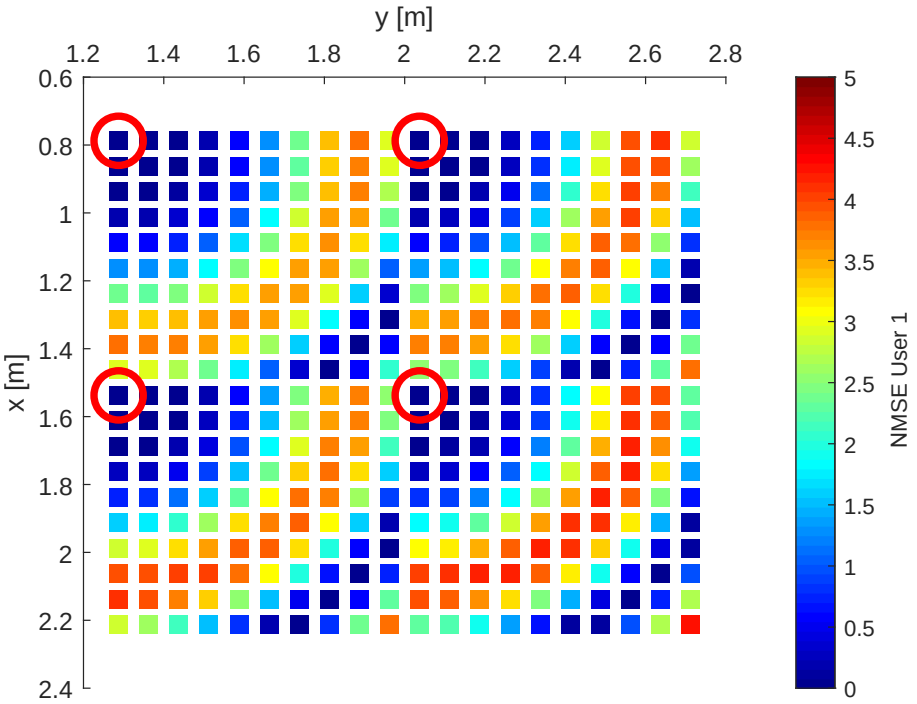

Figure 3.15: NMSE measurements for each antenna in a LIS, considering only a LoS communication scenario with one user at $z = 1$ m, centered with the LIS positioned at $z = 3$ m and divided by $P = 4$ panels, each with $a_p = 100$ antennas, totalling $M = 400$ antennas.

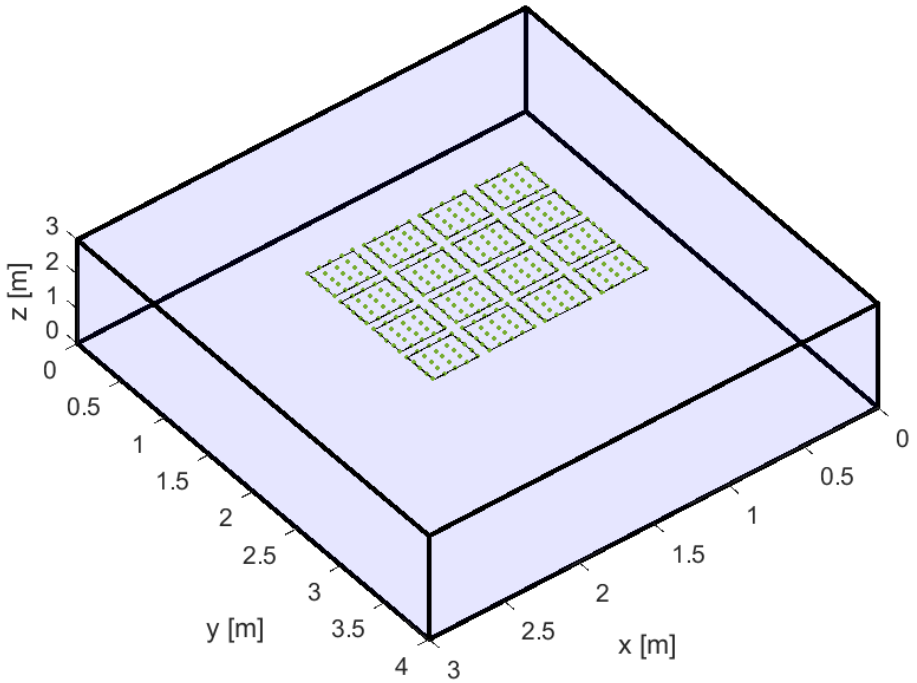

Figure 3.16: Representation of the LIS divided in $P = 16$ panels.

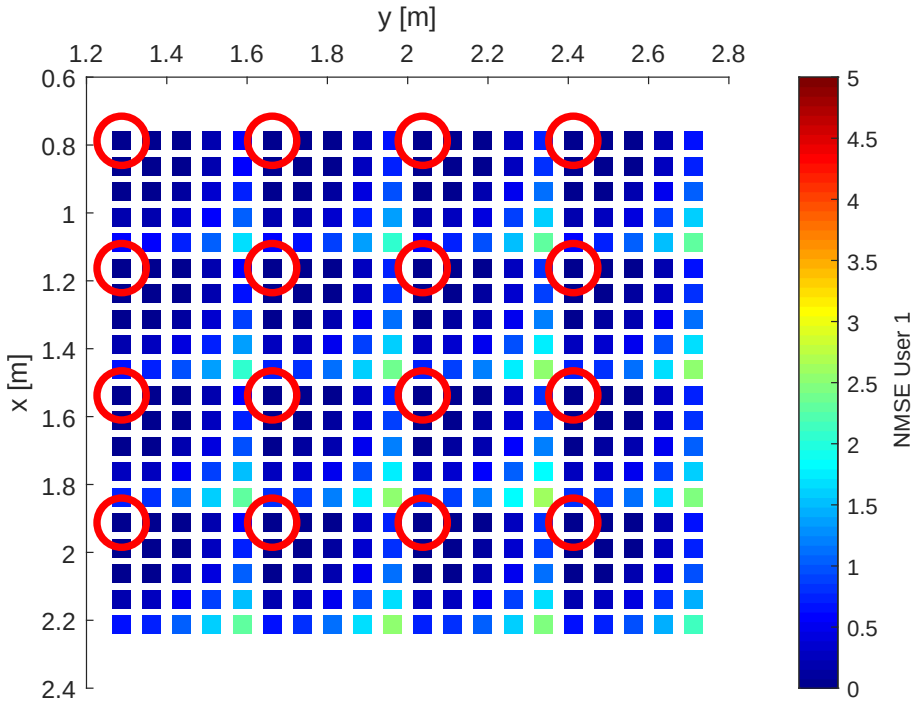

Figure 3.17: NMSE measurements for each antenna in a LIS, considering only a LoS communication scenario with one user at $z = 1$ m, centered with the LIS positioned at $z = 3$ m and divided by $P = 16$ panels, each with $a_p = 25$ antennas, totalling $M = 400$ antennas.

antenna elements, it might be possible to reduce the channel complexity by considering a multi-panel LIS. In such an approach, the use of a single reference antenna per panel might provide accurate estimation results provided that the parallel ray approximation hold.

3.3.2 Scattering Communication Environment

In order to obtain results closer to a real communication environment, let us consider now the same previous scenario in which the ceiling of the indoor room is at $z = 3$ m and it communicates with one user that is centered with the panel at $z = 1$ m, however, it is taken into account both the LoS ray and the reflections associated to the four walls, i.e., $I = 5$, as depicted in figure 3.18.

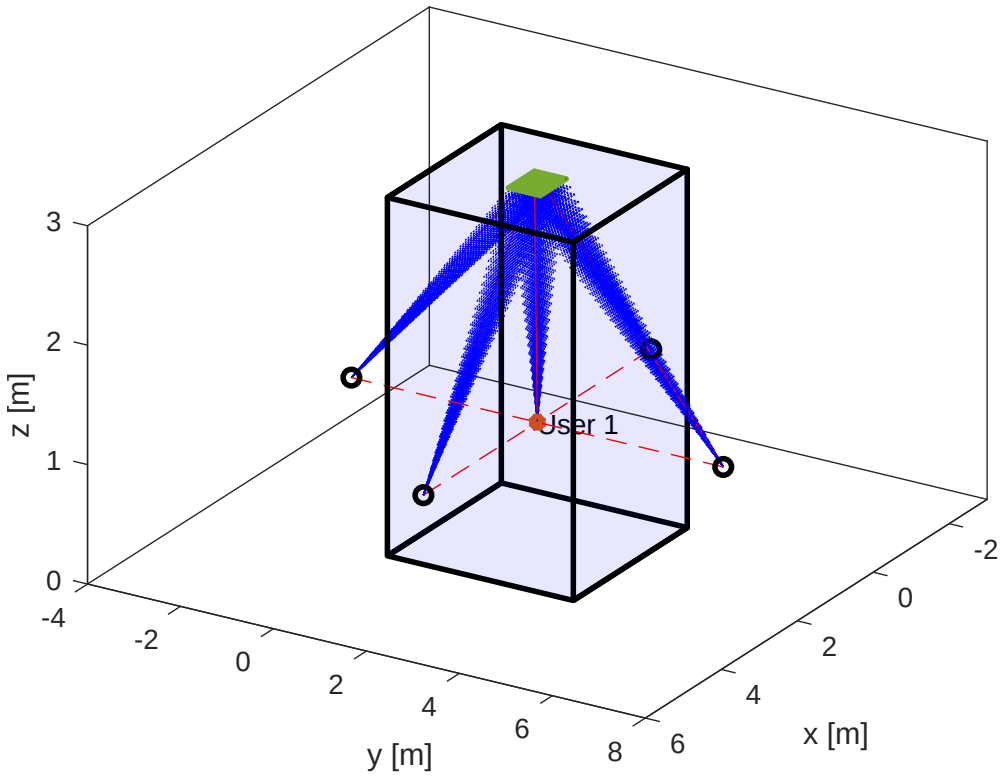

Figure 3.18: Indoor room scattering communication scenario with one user at $z = 1$ m centered with the LIS, which is at $z = 3$ m.

Figure 3.19, considers a LIS with a total of $M = 100$ deployed in a single panel and shows the results of NMSE of the proposed channel estimation technique. Moreover, presents the NMSE resuls for a LIS with $M = 400$ antennas are shown in figure 3.20.

From these figures, it is again possible to observe that the number of antennas for which the channel estimation is not favorable is higher.

Figure 3.21 shows the results of NMSE of the proposed channel estimation technique, for a LIS with a total number of $M = 400$ antennas divided by $P = 4$ panels.

Once again, it can be observed that the channel estimation improves significantly when the number of panels is increased and therefore more reference antennas (one per panel) are used in the estimation process. When considering $M = 400$ antennas divided into $P = 16$ panels, each with $a_p = 25$ antennas (which means that its going to be used only 16 pilots, one per each reference antenna), the results shown in figure 3.22 also sustain this conclusion.

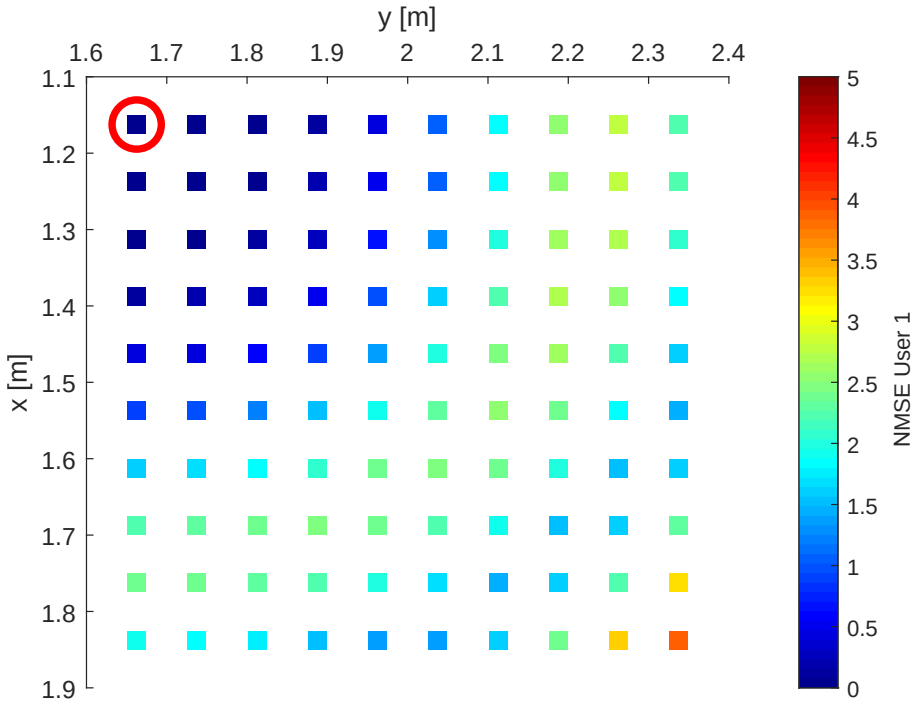

Figure 3.19: NMSE measurements for each antenna in a LIS, considering a scattering communication scenario with one user at $z = 1$ m, centered with the LIS positioned at $z = 3$ m and with $M = 100$ total antennas.

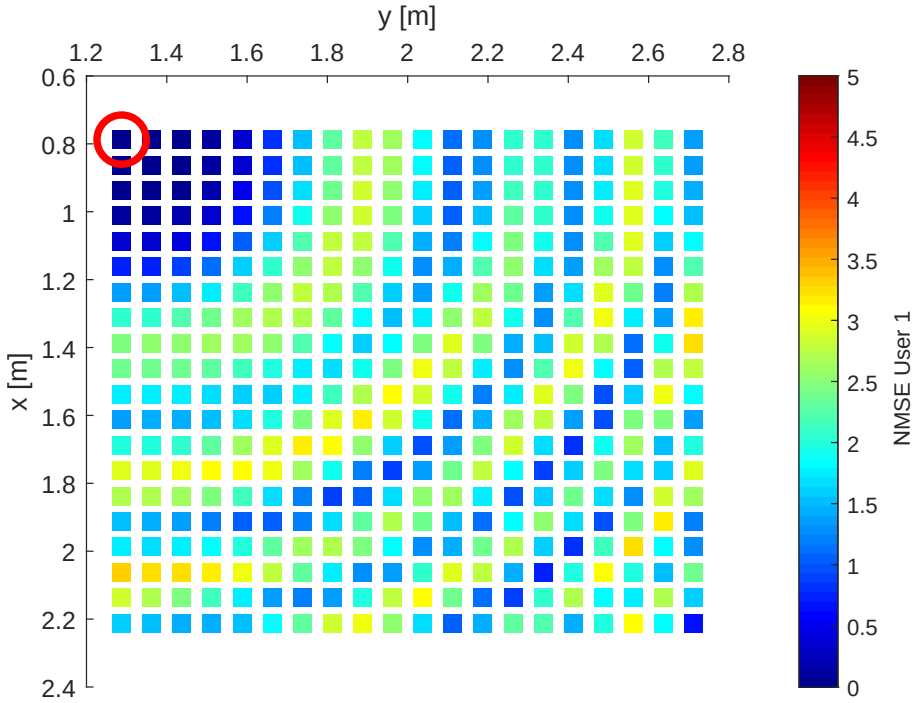

Figure 3.20: NMSE measurements for each antenna in a LIS, considering a scattering communication scenario with one user at $z = 1$ m, centered with the LIS positioned at $z = 3$ m and with $M = 400$ total antennas.

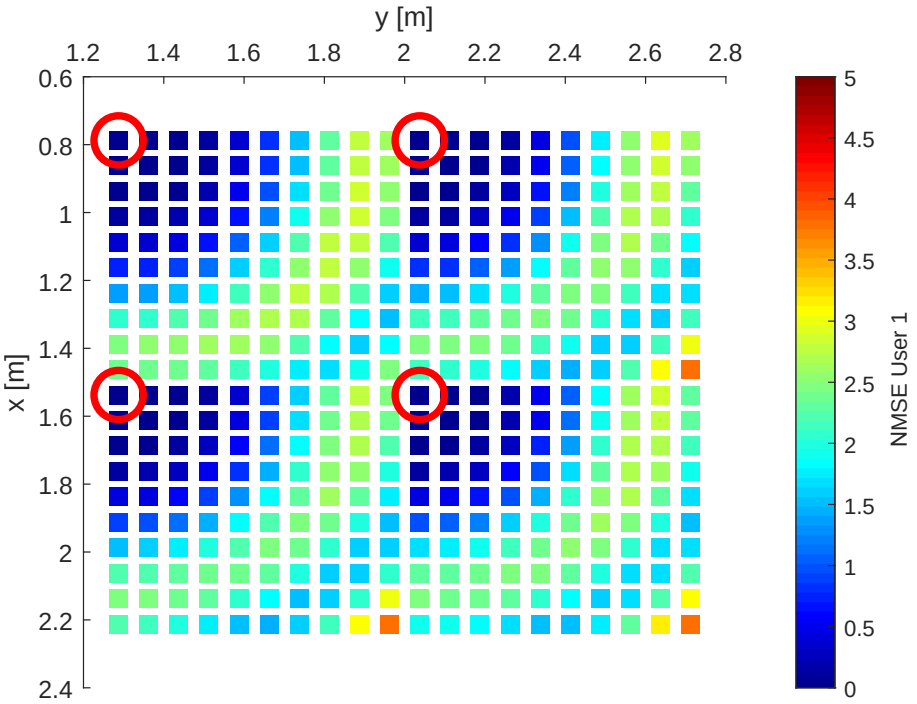

Figure 3.21: NMSE measurements for each antenna in a LIS, considering a scattering communication scenario with one user at $z = 1$ m, centered with the LIS positioned at $z = 3$ m and divided by $P = 4$ panels, each with $a_p = 100$ antennas, totalling $M = 400$ antennas.

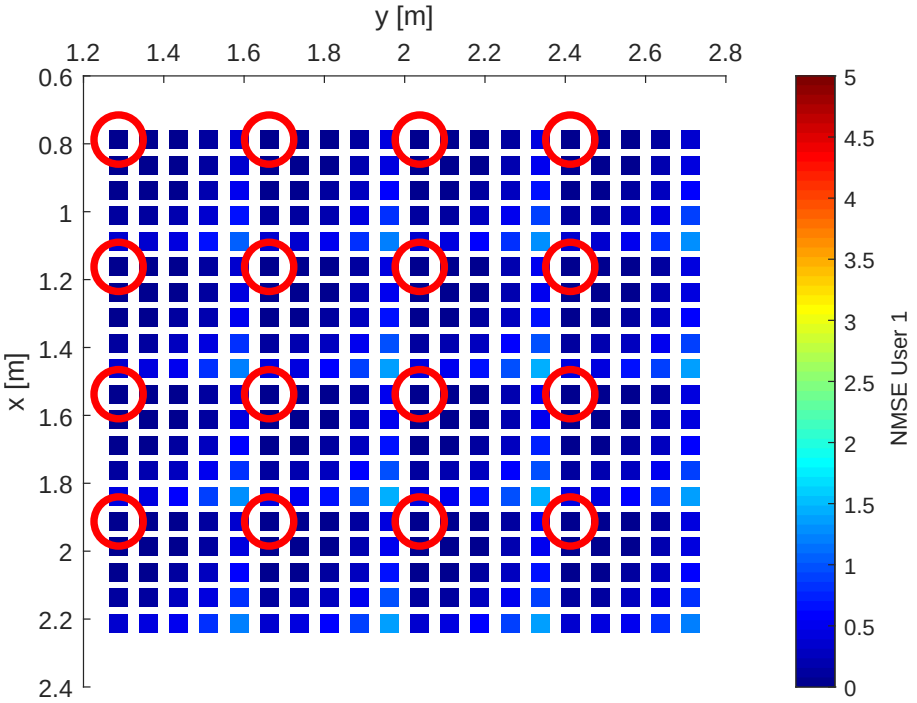

Figure 3.22: NMSE measurements for each antenna in a LIS, considering a scattering communication scenario with one user at $z = 1$ m, centered with the LIS positioned at $z = 3$ m and divided by $P = 16$ panels, each with $a_p = 25$ antennas, totalling $M = 400$ antennas.

3.3.3 Final Remarks & Results Discussion

The obtained simulation results of the NMSE enabled the analysis of the channel estimation performance, which was evaluated considering the presented conceptualized scenarios and in accordance with the explained methodology in the previous sections.

The principal objective was to test a LIS communication system and analyze if the usage of one pilot per panel is suitable to obtain the channels of all remaining antennas of the panel leveraging only the information regarding the AoAs. This goal was achieved by confirming the conceptualized hypothesis.

Additionally, it was also possible to infer other secondary conclusions regarding a LIS communication system from the empirical findings as follows:

- The distance between the UE and the LIS affects directly the extrapolation results, more specifically, the farther the UE is to the LIS, the more accurate the extrapolation process using AoAs is.
- The NMSE values display generally a pattern behavior along the panel of the LIS (i.e., as it gets more distant to the reference antenna), in which the results fluctuate between 0 and 5. Some results showed a consistent and expected decline as the distance increases. However, some other results display a fluctuation pattern that gradually deteriorates and then improves due to the harmonic characteristics of the angles used in the extrapolation process.
- The results obtained are considerably better in a scattering communication scenario when compared with one with only LoS communication.

In summary, the assessment of the performance algorithms allowed us to conclude that a reduction of the channel estimation complexity can be encouraged through the determination of the CIR for only a reduced set of reference antennas and extrapolate the remaining CIRs with that information instead of calculating the CIR for all antennas that comprise a LIS system since it is impractical and time-consuming as previously stated, especially for very large antenna arrays such as the LIS.

4

Low-Complexity Channel Estimation using Spatial Interpolation

This chapter aims to introduce the process and describe the methodology employed in order to obtain a low-complexity channel estimation technique with respect to ELAAs that is based on spatial interpolation. Moreover, to capitalize on the previously addressed theoretical advantages obtained by the employment of RSs, it is fundamental to establish low-complexity channel estimation techniques. For the purpose of accomplishing this objective, the considered communication environment in the following sections incorporates an uplink scenario between a RS and UEs, which communicate through a LoS link.

4.1 System Characterization

A RS is comprised of a substantial amount of antennas in the same manner as a LIS. However, in an RS, antennas are integrated into a single stripe so that a large one dimension antenna array is formed. Due to the large number of antennas involved in a RS, traditional channel estimation techniques become obsolete due to the inherent high level of complexity, costs, and considerable time needed. In that sense, the motivation for using a spatial channel interpolation technique goal is again the reduction of the channel estimation complexity through the use of a reduced number of antennas. As will be described in detail in this section, this technique is formulated on the spatial characteristics of the channel model that characterizes the propagation environment between the RS and UEs.

In the contemplated communication environment of this simulation study, the RS is defined as a straight line with length l_{RS} aligned with the horizontal axis at $y = 0$, as shown in the following figure 4.1. The RS has a total of N isotropic antennas distanced by d_x from each other and is able to communicate with U users through a LoS ray. In other words, it means that a scattering communication scenario was not considered in the simulation study. It is assumed that the RS system is operating in the far-field region with carrier frequency f_c and thus operating with wavelength $\lambda = c/f_c$, with c being the propagation speed of light in vacuum. In table 4.1 is presented an overview of all the

characteristics of the RS system and respective communication environment elements considered in the simulation study.

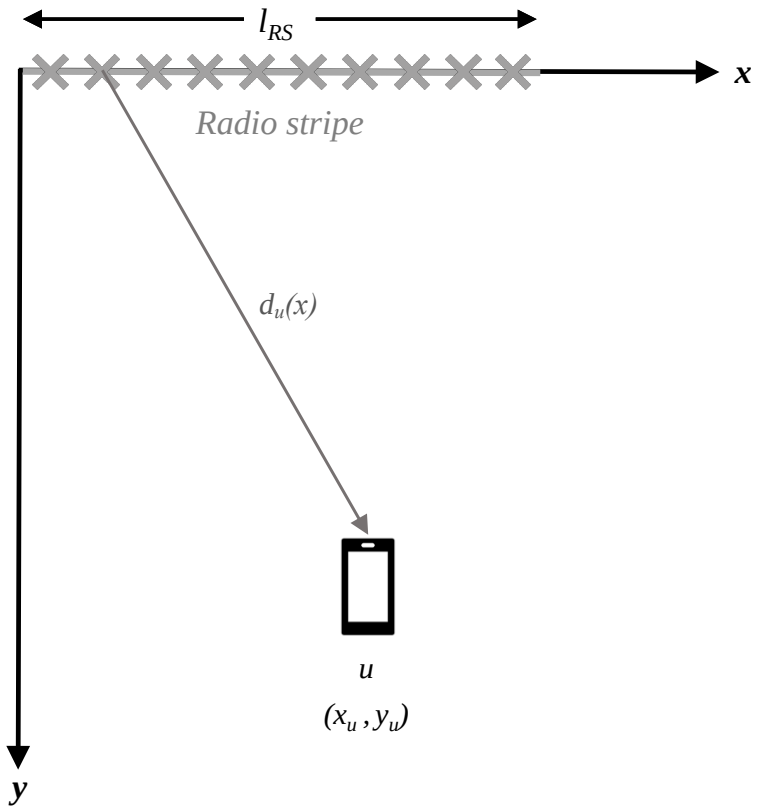

Figure 4.1: Illustrative representation of the conceptualized RS communication scenario.

Parameter	Description
f_c	Carrier frequency
$\lambda = c/f_c$	Wavelength
l_{RS}	Length of the RS
d_x	Distance between antenna elements in the RS
$N = l_{RS}/d_x$	Total number of antennas in the RS
U	Number of users

Table 4.1: Parameters associated with the design of the RS and the communication environment.

4.2 Estimation of the Channel Gain using Discrete Fourier Transform (DFT)

As previously stated, channel modeling has a crucial role that enables the assessment and analysis of the wireless communication system performance. This ongoing section focuses on the methodology employed to compute the propagation channel gain of the considered conceptualized scenario. The main idea is to consider a spatial sampling theorem and obtain the channel gain in a reduced set of antennas. Then, together with a Discrete Fourier Transform (DFT) interpolation, these channel estimates are used to obtain the channel gains of all antennas of the RS.

4.2.1 Channel Gain and Fourier Transform (FT)

Let's assume that the users and the RS communicate in the far-field region and both have isotropic antennas (antennas that radiate equally in all directions with the same intensity), as previously mentioned. Additionally, let us also consider the existence of an antenna in each coordinate x along the RS. Under these conditions, the distance associated with the LoS ray between the uth user and an antenna along the x axis from the RS at $y = 0$ is calculated as follows

$$d_u(x) = \sqrt{(x - x_u)^2 + y_u^2}, \tag{4.1}$$

where x and (x_u, y_u) represent the position of an antenna of the RS and the position of the uth user, respectively. When receiving a signal from the uth user, an antenna of the RS captures the power P_{rx}, accordingly calculated by the following equation

$$P_{rx}(x) = \left(\frac{\lambda}{4\pi d_u(x)}\right)^2 P_{tx}, \tag{4.2}$$

where P_{rx} and P_{tx} are the power received in the antenna and the power transmitted by the uth user, respectively.

Assuming the existence of an antenna in each coordinate x along the RS as indicated before, the baseband complex-valued LoS ray that defines the link between the uth user and an antenna in the RS can be defined as

$$\tilde{\alpha}_u(x) = \sqrt{g_u(x)}\exp(j\theta_u(x)) = \alpha_u(x)\exp(j\theta_u(x)), \tag{4.3}$$

where $g_u(x)$ is the channel gain and $\theta_u(x)$ is the phase, related to the propagation delay. Therefore, the channel gain can be calculated by

$$g_u(x) = |\tilde{\alpha}_u(x)|^2. \tag{4.4}$$

Since we have an antenna in each coordinate x along the RS, we are in the far-field region and we are only considering isotropic antennas, the channel gain along the RS can be described as a "continuous-space" function, respectively,

$$\begin{aligned} g_u(x) = \frac{P_{rx}}{P_{tx}} &= \left(\frac{\lambda}{4\pi d_u(x)}\right)^2 \\ &= \left(\frac{\lambda}{4\pi}\right)^2 \frac{1}{d_u^2(x)} \\ &= \left(\frac{\lambda}{4\pi}\right)^2 \frac{1}{(x-x_u)^2 + y_u^2} \\ &= \frac{\lambda^2}{4} \frac{1}{4\pi^2 y_u^2 + 4\pi^2 (x-x_u)^2} \\ &= \frac{\lambda^2}{16\pi y_u} \frac{4\pi y_u}{4\pi^2 y_u^2 + 4\pi^2 (x-x_u)^2}. \end{aligned} \tag{4.5}$$

Note that by defining $\lambda_u = \frac{\lambda^2}{16\pi y_u}$ and $a_u = 2\pi y_u$ and substituting in the previous equation (4.5), it is possible to rewrite the channel gain as

$$g_u(x) = \lambda_u \frac{2a_u}{a_u^2 + 4\pi^2 (x-x_u)^2}. \tag{4.6}$$

The corresponding FT of (4.6), denoted as $\mathcal{F}(\cdot)$, gives out a signal's spatial frequencies and their respective magnitudes by transforming, as the name suggests, a signal sampled in time or space to an equivalent signal sampled in temporal or spatial frequency. Therefore, with the goal of calculating the FT of $g_u(x)$, let's define

$$g_u(x) = g'_u(x - x_u), \tag{4.7}$$

which means that

$$g'_u(x) = \lambda_u \frac{2a_u}{a_u^2 + 4\pi^2 x^2}. \tag{4.8}$$

Under these conditions, the FT of $g'_u(x)$ is calculated by the following equation

$$G'_u(\nu) = \mathcal{F}(g'_u(x)) = \lambda_u \exp(-a_u|\nu|), \tag{4.9}$$

where ν is the variable of the FT that corresponds to the "spatial frequency" which is measured in units of m^{-1}.

By considering the change of variable and the translation property of the FT, it can be obtained the FT of the real channel gain, which is given by

$$G_u(\nu) = \mathcal{F}(g'_u(x - x_u)) = G'_u(\nu)\exp(-j2\pi\nu x_u). \tag{4.10}$$

In order to obtain the distribution of the power over the spatial frequency associated with $G_u(\nu)$, it is first calculated the Power Spectral Density (PSD) as follows

$$W_u(\nu) = |G_u(\nu)|^2 = \lambda_u^2 \exp(-2a_u|\nu|). \tag{4.11}$$

By considering (4.11) it is finally possible to obtain the total power of $G_u(\nu)$, which is given by the following equation

$$P_u = \int_{-\infty}^{\infty} W_u(\nu)d\nu = \lambda_u^2 \int_{-\infty}^{\infty} \exp(-2a_u|\nu|)d\nu = 2\lambda_u^2 \int_0^{\infty} \exp(-2a_u\nu)d\nu = \frac{\lambda_u^2}{a_u}.$$

4.2.2 Nyquist Sampling Theorem

As previously introduced, it was used a spatial interpolation method with the purpose of obtaining a low-complexity channel estimation technique concerning a RS system. This channel estimation technique is based on the Nyquist theorem also known as the sampling theorem. This theorem is a fundamental theoretical principle and states that for a function that is band-limited to a given bandwidth B, it is possible to perfectly reconstruct the original continuous-time function from samples in such a manner that no actual information is distorted or lost. In addition, to ensure perfect reconstruction the $f_s \geq 2B$ criterion, where f_s is the sampling frequency, must be complied with and a suitable filtering process must be performed. When such conditions are not met (i.e., $f_s < 2B$), the signal reconstruction exhibits imperfections giving rise to an effect known as aliasing.

However, in this developed environment there are no time-domain signals or their frequency-domain version. Instead, there are signals that are functions of x, hence defined in the spatial domain, measured in m (meters) and the respective FTs that are functions of ν, therefore the "spatial frequency" domain, measured in m^{-1}. That being the case, the equivalent "discrete-space" FT of the samples is computed by

$$G_P(\nu) = \sum_{k=-\infty}^{\infty} G(\nu - kf_s). \tag{4.12}$$

In a realistic communication scenario, the RS is not going to have an antenna in each coordinate x along the stripe and it will be confined to a certain length. However, this length can be several meters long and have a multitude of antennas which makes the task

of channel estimation very complex. Therefore, the objective of the proposed technique is to use the spatial sampling theorem to reduce the number of antennas that need to be considered in the estimation process.

In a RS of finite bandwidth with length l_{RS} exists a total of N antennas, determined by

$$N = \frac{l_{RS}}{d_x}, \tag{4.13}$$

and can be represented by a set of equidistant sampling points separated by

$$d_s = S \times d_x, \tag{4.14}$$

where d_x is the distance between antenna elements in the RS, as stated before. Note that in order to reduce the complexity of the channel gain estimation process, it is considered that the number of the sample antennas N_s must be lower than the total number of antennas, N (i.e., $N_s < N$,), in the RS. By using the DFT interpolation we can then interpolate the channel for the remaining $N - N_s$ antennas, thus it is implicitly assumed that $d_s \geq d_x$. Additionally, for a given sampling ratio of $S = N/N_s$ antennas, the indirect spatial sampling frequency, which is defined as f_s, can be calculated by

$$f_s = \frac{1}{d_s} = \frac{1}{S \times d_x}. \tag{4.15}$$

The spatial sampling process that characterizes the methodology employed in this study can be observed in the following figure 4.2.

It should be noted that the definition of S can be made according to the "spatial" bandwidth of the channel gain along the RS. This is explained by the fact that S acts like a sampling spacing, just like the conventional time-domain sampling theorem where if the spacing between samples is higher, the interpolation (i.e., reconstruction) quality can be worse.

By taking into consideration only the N_s antennas used for the channel estimation, let us define a vector, denoted by $\mathbf{g}_{u,s}$, that comprises the channel gains previously computed in the equation (4.6)

$$\mathbf{g}_{u,s} = [g_{u,s_1}\ g_{u,s_2}\ \cdots g_{u,s_n}]. \tag{4.16}$$

Note that these estimates can be obtained through pilot symbols. In the remaining of this chapter, it is assumed that the channel of the antennas used in the interpolation process is perfectly known.

The objective is to use the samples of $\mathbf{g}_{u,s}$ (where each sample is a channel gain) to estimate the channel gain for all N antennas, that will compose the following vector

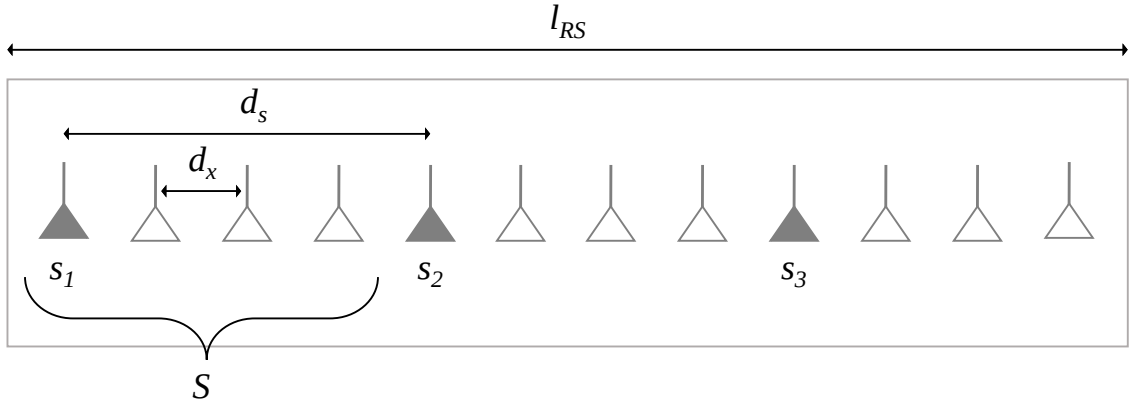

Figure 4.2: Illustrative representation of a RS with $N = 12$ antennas and the respective variables l_{RS}, d_x, d_s and S used in the proposed method. In this case, $S = 4$ and therefore, $N_s = 3$.

$$\hat{\mathbf{g}}_{u,a} = [\hat{g}_{u,a_1}\ \hat{g}_{u,a_2}\ \cdots \hat{g}_{u,a_n}], \tag{4.17}$$

With the purpose of accomplishing this whilst enhancing computational efficiency, it is computed the DFT of $\mathbf{g}_{u,s}$, which is denoted by $\mathbf{G}_{u,s} = \text{DFT}(\mathbf{g}_{u,s})$. This mathematical concept provides the necessary tools to represent in a simpler manner a finite length sequence using a periodic sequence, i.e. a given sample set of S antennas, meaning that one period of this sequence will be used to interpolate and obtain the finite length sequence considered. Subsequently, it is calculated the Inverse Discrete Fourier Transform (IDFT) of a zero-padded DFT (with $N - N_s$ zeros), so that the interpolation is made and the channel gain for all antennas can be obtained. Accordingly, the zero padding of the DFT of $\mathbf{g}_{u,s}$ will enable a more accurate estimation of the signal components.

In order to evaluate the efficiency of the proposed interpolation technique, it is important to define the MSE of the channel gain estimates, in such a manner that the estimation error can be measured. Accordingly, the MSE is computed as follows

$$\text{MSE} = \frac{\|\mathbf{g}_{u,a} - \hat{\mathbf{g}}_{u,a}\|^2}{\|\mathbf{g}_{u,a}\|^2}. \tag{4.18}$$

4.3 Performance Results

In this section, it is provided the obtained simulation results that enable the evaluation and analysis of the channel gain estimation performance, having as foundation and support the methodology explained in the previous sections 4.2.1 and 4.2.2.

This ongoing section is organized as follows: in subsection 4.3.1 it is first presented a study regarding the channel gain in its broader sense. Then, in the following subsection

4.3.2 it is introduced a more detailed analysis concerning the direct application of the proposed technique along the RS, considering different sampling ratios. Finally, subsection 4.3.3 contains a summary of the main conclusions drawn from the performed simulations.

4.3.1 Channel Gain

Let us start by assuming a communication scenario in which the RS has an infinite length ($l_{RS} = \infty$) and is placed at the horizontal axis. This RS communicates with two users ($U = 2$) which are positioned at $(x_u, y_u) = (5, 10)$ and $(x_u, y_u) = (20, 6)$, respectively.

Fig. 4.3 shows the evolution of the channel gain along a limitless RS with $U = 2$ users located in different positions.

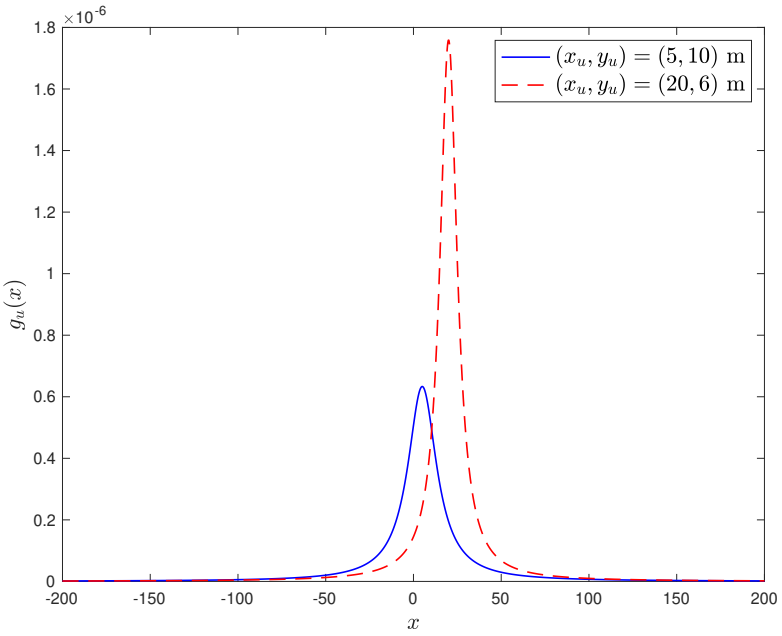

Figure 4.3: Evolution of the channel gain along a limitless RS with $U = 2$ users located in different positions.

As can be noted from the figure, the channel gain, denoted as $g_u(x)$, reaches its peak when $x = x_u$ which corresponds to the point where the distance between the user and an antenna of the RS is minimal, in accordance with equation (4.1). Additionally, the channel gain peak is higher the closer the user is to the RS vertically.

Let us now consider the spatial frequency domain of the channel gain for the scenario of figure 4.3. Figure 4.4 shows the evolution the absolute value of the channel gain's spatial frequency version along the RS (i.e., the absolute value of the FT of the channel gain previously calculated in equation (4.10)).

Accordingly, when considering a RS with infinite length, it is possible to infer that the evolution of $|G_u(\nu)|$ only depends on the vertical distance between the users and

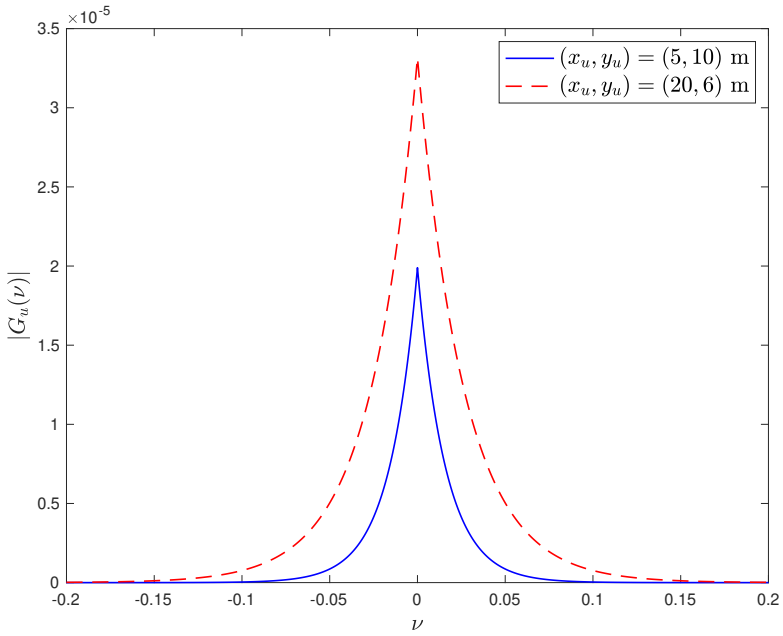

Figure 4.4: Spatial frequency-domain channel gain considering $U = 2$ users located in different positions.

the antennas, which suggests that the spatial bandwidth is only dependent on the y coordinate of the users.

Now let us consider a communication scenario where the RS, defined previously as a straight line aligned with the horizontal axis at $y = 0$, has now $l_{RS} = 10$ m, starting at $x = 0$, and a spacing between antennas of $d_x = \lambda/10$. Therefore, according with the equation (4.13), the RS has $N = 1000$ total antennas. These antennas communicate with $U = 3$ users in different positions.

As can be seen from figure 4.5, the channel gain progression is now a truncated and discrete version of $g_u(x)$. Therefore, in a more realistic scenario where the RS has a finite length, both coordinates of the user position (i.e. (x_u, y_u)) have an influence on the channel gain progression along the RS. Moreover and reinforcing these insights, figures 4.6 and 4.7 show the effect that the users' position on the evolution of the channel gain.

As can be noted as users move out from the perpendicular to the RS, the channel gain losses the symmetry. In terms of spatial frequency, this might lead to large bandwidths and difficulties in the interpolation process.

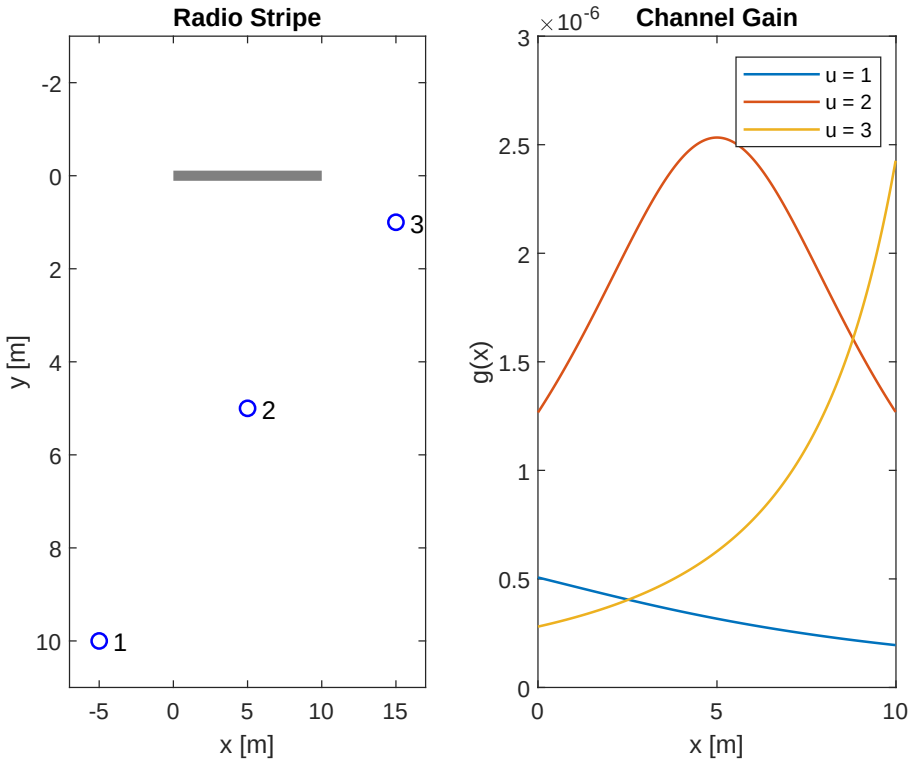

Figure 4.5: Communication scenario where a RS with $l_{RS} = 10$ m serving $U = 3$ users located in different positions (on the left figure) and evolution of the channel gain for each respective users (on the right figure).

4.3.2 Channel Gain Estimation with Different Sampling Ratios

With the purpose of reviewing the channel gain estimation performance with the technique demonstrated in the previous section 4.2, let us consider once again the last communication scenario depicted, where a RS is aligned with the horizontal axis, has $l_{RS} = 10$ m and spacing between antennas of $d_x = \lambda/10$ (thus $N = 1000$ total antennas). However, in the following scenarios, unless stated otherwise, it is considered that each antenna in the RS only communicates with a single user ($U = 1$). Additionally, depicted by a black solid line is the real channel gain, meaning that $S = 1$. On the other hand, represented by dashed lines are the recovered channel gains each with different sampling ratios, $S = \{25, 50, 100, 200\}$ respectively.

Figure 4.8 shows a scenario in which the RS communicates with a user positioned at $(x_u, y_u) = (5, 5)$, centered with the stripe.

From the figure, it can be noted that the recovered channel gain deviates slightly from the real channel gain, which represents a positive performance, and only starts to deviate in a more accentuated manner at the RS limits. Additionally, it is observed that when the sampling ratio S increases, the deviations to the real channel gain ($S = 1$) also increase accordingly. This is expected since the higher the value of S, the lower the number of effective antennas used in the interpolation process and the lower the estimation performance.

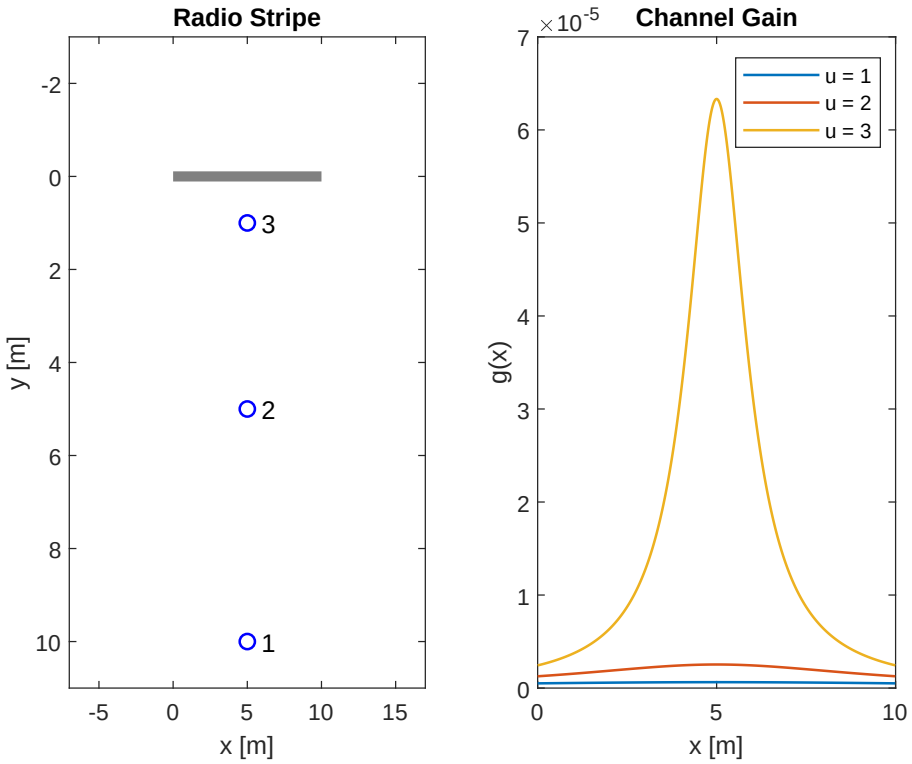

Figure 4.6: Communication scenario where a RS with $l_{RS} = 10$ m serving $U = 3$ users located in different positions and aligned vertically (on the left figure); and evolution of the channel gain for each respective users (on the right figure).

In figure 4.9, the user is once again centered with the RS but farther away from it, at $(x_u, y_u) = (5, 10)$ m.

From the figure, one can observe that the recovered channel gains deviate increasingly when reaching both edges of the RS. Moreover, it can be noted that in this scenario, the deviation between the recovered channel gain and the real channel gain is more accentuated when considering $S = 200$, especially at the peak of the curve.

Let us now consider that the user moves to the edge of the RS. Figures 4.10 and 4.11 showcase two communication scenarios between the RS and a user positioned at $(x_u, y_u) = (10, 10)$ and $(x_u, y_u) = (10, 2)$, respectively.

From these figures, it can be once again confirmed that the estimation performance deteriorates accordingly as we reach both limits of the RS and as the sampling ratio S increases. It is also possible to infer that when comparing with the results in figures 4.8 and 4.9 (in which the user is centered with the RS), the deviation between the channel gains is slightly noticeable.

Furthermore, let us now consider a scenario in which the RS communicates with users positioned in a grid around the RS. Figure 4.12 is an illustrative example of this scenario, taking into consideration different sampling ratios S.

Moreover and with respect to the former figure 4.12, the following figure 4.13 exhibits the channel gain estimation performance, i.e. the MSE of the estimations, considering

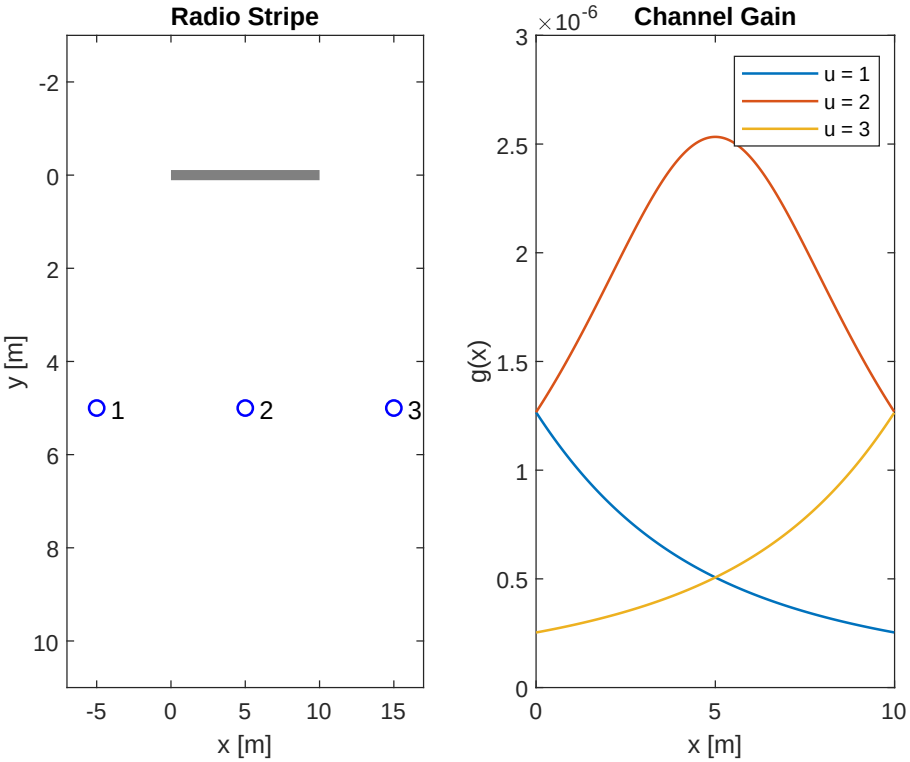

Figure 4.7: Communication scenario where a RS with $l_{RS} = 10$ m serving $U = 3$ users located in different positions and aligned horizontally (on the left figure); and evolution of the channel gain for each respective users (on the right figure).

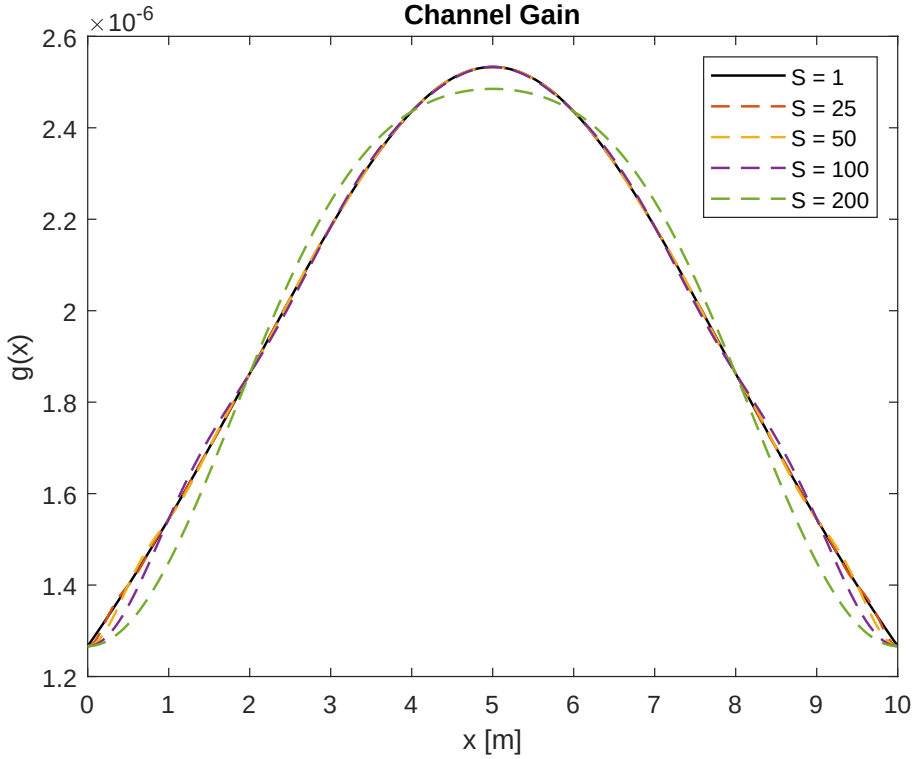

Figure 4.8: Representation of the channel gain evolution along the RS for a user positioned at $(x_u, y_u) = (5, 5)$ considering different sampling ratios S.

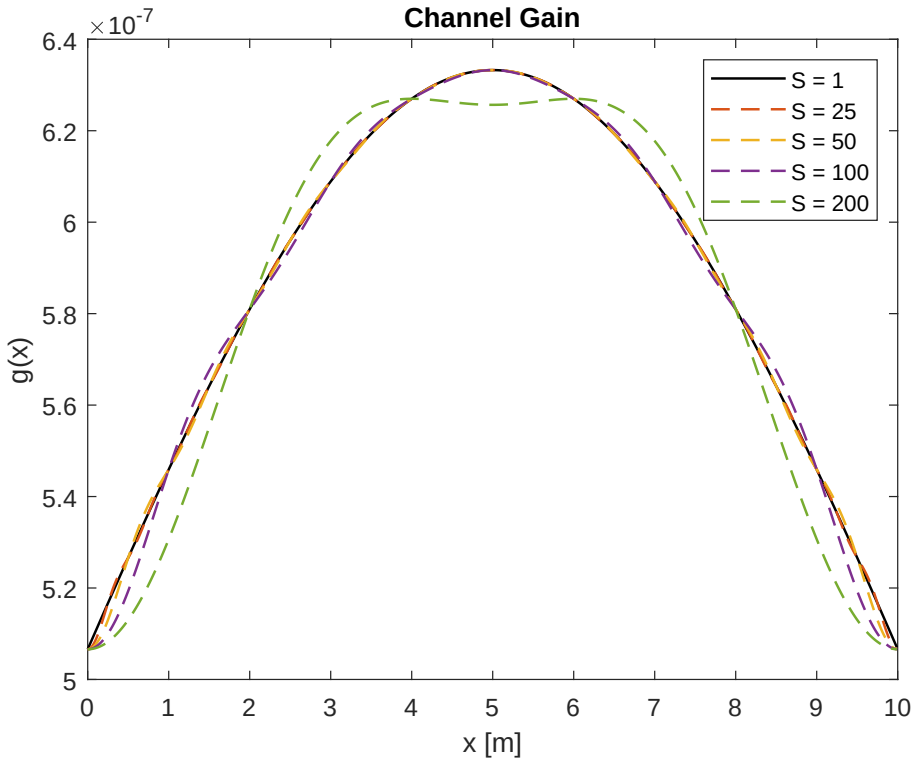

Figure 4.9: Representation of the channel gain evolution along the RS for a user positioned at $(x_u, y_u) = (5, 10)$ considering different sampling ratios S.

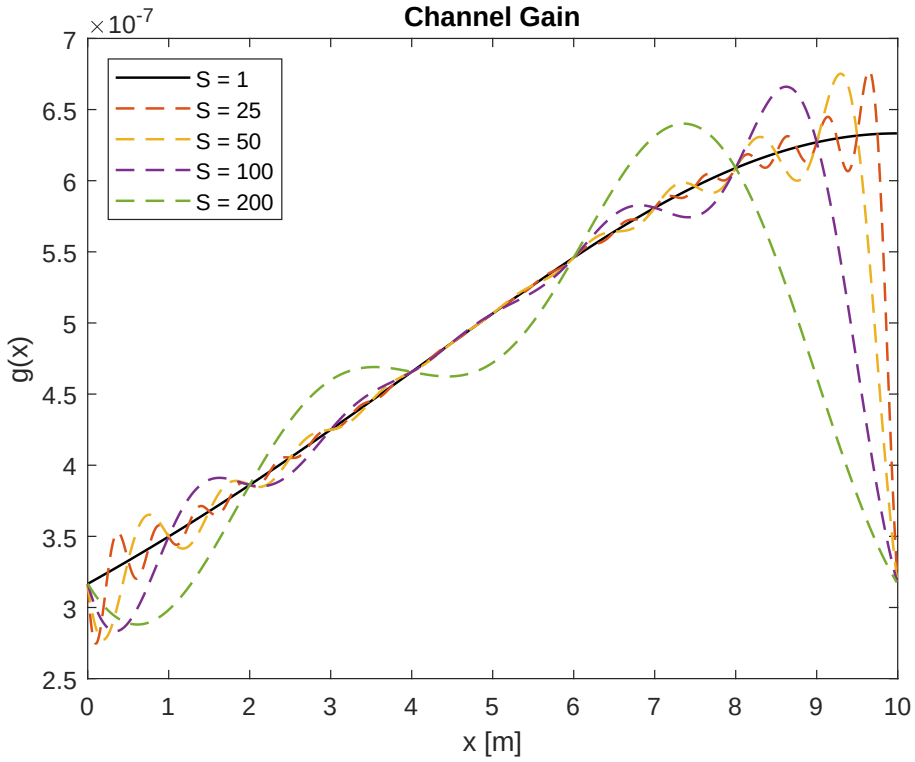

Figure 4.10: Representation of the channel gain evolution along the RS for a user positioned at $(x_u, y_u) = (10, 10)$ considering different sampling ratios S.

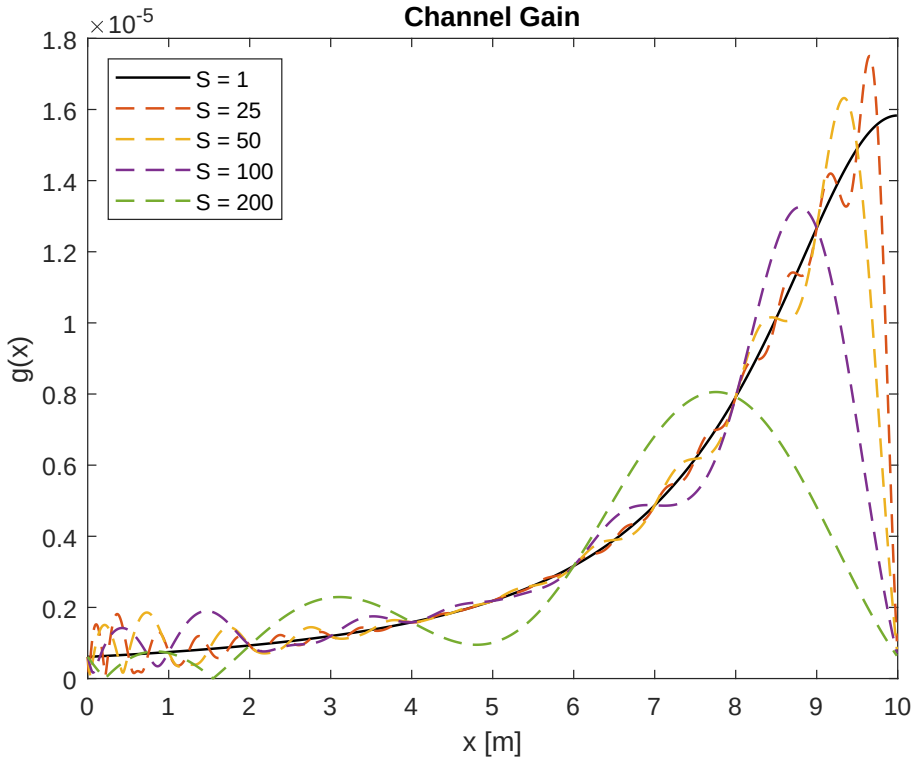

Figure 4.11: Representation of the channel gain evolution along the RS for a user positioned at $(x_u, y_u) = (10, 2)$ considering different sampling ratios S.

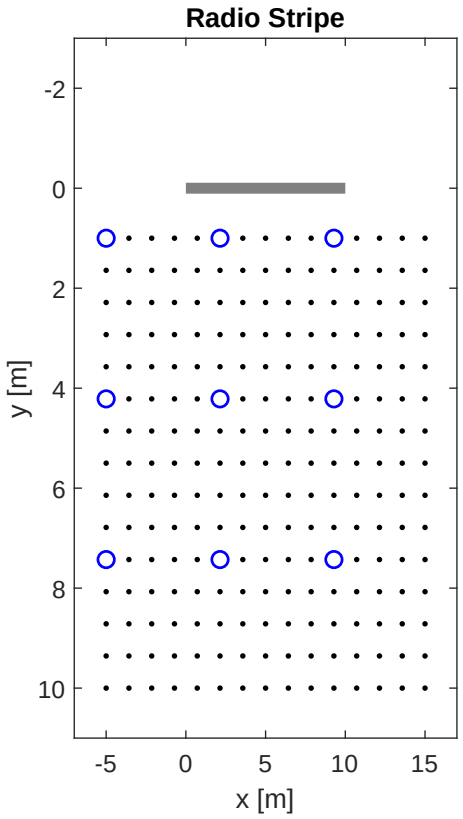

Figure 4.12: Illustrative representation of a communication scenario in which the RS communicates with users positioned in a grid.

the same sampling ratios as in figures 4.8 to 4.11 ($S = \{25, 50, 100, 200\}$).

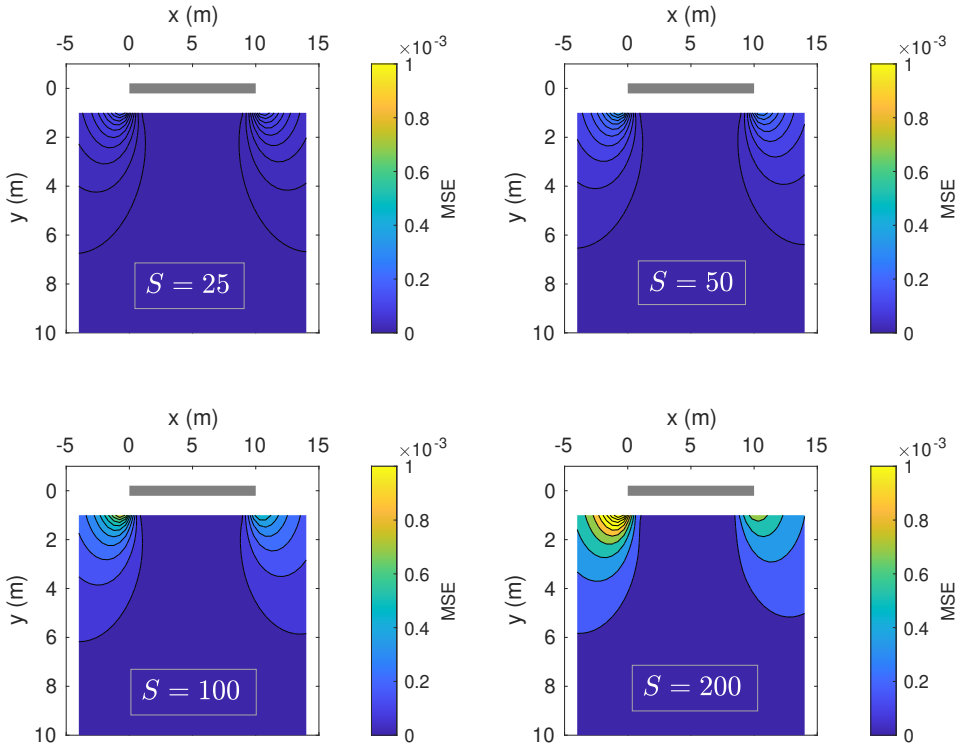

Figure 4.13: MSE measurements of the channel gains estimates considering different values of S.

From these results, it can be noted that this channel gain estimation technique performs quite well, i.e., it is able to achieve lower MSE values. As observed previously, as the sampling ratios increase so does the MSE and, additionally, for each sampling ratio, the performance hinders when reaching the edges of the RS. Also, is important to highlight that the results obtained and showcased in figure 4.13 give even more emphasis to the positive performance of the estimation technique when an user is positioned in any point along the RS in the x axis, in this case between 0 and 10 meters, no matter the value of the sampling ratio.

4.3.3 Final Remarks & Results Discussion

The empirical findings inferred from the realized simulations contributed to the analysis of the channel estimation performance of this spatial interpolation technique. In addition, this analysis was carried out taking into consideration the provided methodology in section 4.2 and the previous scenarios conceptualized in subsections 4.3.1 and 4.3.2.

The main goal was to use the spatial characteristics of the channel gain of specific antennas in a RS communication scenario, to interpolate and obtain the channel gain of other antennas that compose the stripe, namely by considering the spatial domain version of the channel gains and DFT interpolation. The obtained results provide evidence of this method's efficiency when calculating accurately the channel gain estimates along the RS considering only specific antennas in the estimation technique, i.e., when using a low number of pilots.

Even though this technique is successful when it comes to channel gains estimates, the next goal should be using this technique to calculate additionally the CIR, which requires thorough simulations. This can also serve as the basis for improved estimation techniques that can take advantage of the PSD and the bandwidth of the spatial channel gain to calculate the adequate sampling ratio for each use case, depending on the respective user position or per region of the RS. This would allow for a balance between performance and estimation overhead, which is dependent on the number of pilots involved in the estimation process).

Nonetheless, this method proves that it is possible to reduce the complexity of the channel estimation process in ELAAs systems by reducing the necessary number of antennas that need to be considered in the overall estimation process.

5

Conclusions

In the preceding chapters it was introduced the main antenna systems of the current networks and the emerging user requirements for the next generations of wireless systems. Moreover, by means of a thorough study, it was explored the relevance of MIMO and mMIMO systems, since they form the basis of the recently proposed antenna technologies for 6G. As previously outlined in chapter 2, although MIMO systems have immense potential they still face some drawbacks and limitations. Namely, the fact that MIMO systems have a considerable amount of antennas, therefore requiring a substantial increment in transceiver hardware and accordingly, which should have low complexity and be energy efficient. Moreover, improved digital signal processing techniques should also be developed. In this regard, mMIMO is a breakthrough technology. Nonetheless, there is still room for improvement. The new ELAAs concepts, namely LISs, RSs and IRSs, build upon mMIMO and represent a visionary approach towards the demands of future wireless communications.

LIS is a scaled-up version of the current massive MIMO systems and is characterized by its large and thin surface that comprises a considerable number of antenna elements. Moreover, one particular aspect of such systems is their massive dense antenna array that supports the capability of transmitting and receiving radio signals across the LIS entire surface. RS is a stripe that incorporates a substantial amount of serially located antennas. It possesses a flexible cell-free architecture that enables not only its scalability proficiency but also reduces the overall associated costs. IRS is a surface that encompasses numerous small, low-cost passive reflecting elements, each being separately able to control the amplitude and phase of the incident signal. Thus, IRSs can ideally achieve a precise reflect beamforming passively, i.e., without the need for a dedicated energy source for signal processing.

Although promising, there are challenges to be addressed for future practical implementations with ELAAs systems, particularly when it comes to channel estimation tasks and their associated complexity. Respectively, when is composed by a BSs with a large number of antennas and is serving multiple UEs, estimating all the channels for all the TX and RX antennas become unreasonable for the system efficiency. For this reason, in order

to handle greater sum throughput and demands, new low-complexity channel estimation techniques should be developed, so as the benefits of using ELAAs can be fully exploited. Therefore, the aim of this thesis was to further assess and analyze in detail channel estimation techniques that introduce a low-complexity solution to the channel estimation task. In this ongoing chapter, it is provided an overview of key challenges and possible improvements with respect to channel estimation for ELAAs systems regarding this new antenna systems concepts, built on the results presented in the previous chapters 3 and 4.

Accordingly, in chapter 3 it was presented a low-complexity channel estimation technique for ELAAs systems based on spatial information. It was created a geometric model that characterizes a propagation environment of an uplink communication between a LIS system and an UEs in a small indoor room. Additionally, the propagation channel of the considered environment was derived using a ray-tracing technique based on the optics geometry. More concretely the image method approach was considered to derive the CIR and the channel frequency response. This proposed technique takes advantage of a LIS panel-based architecture. Therefore, in order to obtain the channel estimation of all antennas of the LIS, it was first estimated the channel in one antenna of a given panel and only after the remaining channels of that panel were extrapolated, taking into consideration the information concerning the AoAs. The research findings of the various simulation scenarios show that the NMSE is directly affected by the relative position of antennas towards the reference antenna, meaning that the NMSE worsens as the distance to the reference antenna increases. Also, the fact that the NMSE depends on the position of the user to the LIS and exhibits improved results if the user is more distant from the LIS panel. Most importantly, it was proven that the complexity of channel estimation for a LIS system with a large number of antennas can be reduced significantly by calculating the CIR of a chosen reference antenna and extrapolating the CIR of the remaining antennas using only information about the AoAs.

In chapter 4 it was demonstrated the developed low-complexity channel estimation technique for a RS system based on spatial interpolation. It was considered a geometric model that characterizes a propagation environment in an uplink communication between a RS system and an UEs. In the interest of obtaining the channel gain estimation of the entire RS, it was used the estimated channel gains of a sampled number of antennas (where pilots were used) and only then, by using the spatial characteristics of the channel, it was estimated the channel gain for all the remaining antennas of the RS using a DFT interpolation. The research findings of the diverse considered simulation scenarios confirm that several factors can affect the performance of the spatial interpolation method including the user position, the spatial bandwidth, and the sample spatial distribution. Moreover, as expected, the results are directly affected by the sampling ratio considered for the RS system model. Taking everything into account, it was again validated that the channel estimation complexity for an ELAA system, in this case, a RS, with a vast amount of antenna elements can be reduced considerably through the estimation of the

channel for a particular sample set of antennas and then obtaining the channel gain for the remaining antennas.

As a final remark, it is possible to conclude from the obtained results that having an effective channel estimation technique in wireless communications systems is highly important for the quality of the overall system. Therefore, these new ELAAs systems need to secure efficient low-complexity channel estimation techniques that allow for their mainstream practical implementation and accordingly deliver robust and consistent results. In that sense, the reduction of the channel estimation complexity is essential to reduce the overall system complexity as well as to enable faster communications (with low latency), lower overhead costs, and simplified resource allocation techniques.

Additionally, it is important to note some limitations and constraints regarding this study, namely the fact that both channel estimation techniques assumed ideal scenarios with isotropic antennas in both the ELAAs systems and in the UEs, as well as communication in the far-field region with no obstacles in between and without considering user interference. Therefore, in future research, more realistic scenarios should be taken into consideration in such a way that the methods' applicability rises considerably. Moreover, with respect to the estimation technique presented in chapter 4, future work should consider the additional estimation of the CIR of each antenna in the RS as well as using the PSD and the bandwidth. This will allow to achieve greater levels of automation and optimization in the estimation process (for e.g., automatically calculate the adequate sampling ratio for a specific communication scenario), in order to fulfill the theoretical and promising expectations of a RS system.

Nevertheless, the proposed channel estimation techniques demonstrated that the reduction of the complexity is attainable while assuring an adequate performance, thus supporting an effective and prosperous advancement of ELAAs systems on real-world implementations.

Bibliography

[1] E. Basar. "Reconfigurable Intelligent Surface-Based Index Modulation: A New Beyond MIMO Paradigm for 6G". In: *IEEE Transactions on Communications* 68.5 (2020), pp. 3187–3196. DOI: 10.1109/TCOMM.2020.2971486 (cit. on p. 11).

[2] E. Basar. "Transmission through large intelligent surfaces: A new frontier in wireless communications". In: *2019 European Conference on Networks and Communications (EuCNC)* (2019), pp. 112–117. DOI: 10.1109/eucnc.2019.8801961 (cit. on p. 10).

[3] E. . Bjornson and L. . Sanguinetti. "Power Scaling Laws and Near-Field Behaviors of Massive MIMO and Intelligent Reflecting Surfaces". In: *IEEE Open Journal of the Communications Society* 1 (2020), pp. 1306–1324. DOI: 10.1109/ojcoms.2020.3020925 (cit. on pp. 13, 14).

[4] E. Björnson, E. G. Larsson, and T. L. Marzetta. "Massive MIMO: ten myths and one critical question". In: *IEEE Communications Magazine* 54.2 (2016), pp. 114–123. DOI: 10.1109/MCOM.2016.7402270 (cit. on pp. 15, 16).

[5] E. . Björnson, J. . Hoydis, and L. . Sanguinetti. *Massive MIMO Networks: Spectral, Energy, and Hardware Efficiency (Foundations and Trends(r) in Signal Processing)*. Now Publishers Inc, 2018 (cit. on pp. 1, 6–8, 15–17, 25).

[6] B. Choudhury et al. "Comparison of image method and refined ray tracing method for aircraft cabin application". In: *Proceedings of the 2012 IEEE International Symposium on Antennas and Propagation*. 2012, pp. 1–2. DOI: 10.1109/APS.2012.6349082 (cit. on p. 21).

[7] *Cisco Annual Internet Report (2018–2023) White Paper*. Jan. 23, 2022. URL: https://www.cisco.com/c/en/us/solutions/collateral/executive-perspectives/annual-internet-report/white-paper-c11-741490.html (cit. on pp. 1, 2).

[8] D. Dardari. "Communicating With Large Intelligent Surfaces: Fundamental Limits and Models". In: *IEEE Journal on Selected Areas in Communications* 38.11 (2020), pp. 2526–2537. DOI: 10.1109/JSAC.2020.3007036 (cit. on pp. 13, 14).

[9] F. Dong et al. "High-Resolution Angle-of-Arrival and Channel Estimation for mmWave Massive MIMO Systems With Lens Antenna Array". In: *IEEE Transactions on Vehicular Technology* 69.11 (2020), pp. 12963–12973. DOI: 10.1109/TVT.2020.3016671 (cit. on p. 25).

[10] O. Elijah et al. "A Comprehensive Survey of Pilot Contamination in Massive MIMO—5G System". In: *IEEE Communications Surveys Tutorials* 18.2 (2016), pp. 905–923. DOI: 10.1109/COMST.2015.2504379 (cit. on pp. 15, 16).

[11] E. . Ernfors et al. *Radio Stripes – Ericsson*. 2019. URL: https://www.ericsson.com/en/blog/2019/2/radio-stripes (cit. on p. 10).

[12] F. A. P. de Figueiredo et al. "On channel estimation for massive MIMO with pilot contamination and multipath fading channels". In: *2016 8th IEEE Latin-American Conference on Communications (LATINCOM)*. 2016, pp. 1–4. DOI: 10.1109/LATINCOM.2016.7811581 (cit. on p. 17).

[13] H. Friis. "A Note on a Simple Transmission Formula". In: *Proceedings of the IRE* 34.5 (1946), pp. 254–256. DOI: 10.1109/JRPROC.1946.234568 (cit. on p. 23).

[14] S. Hu, F. Rusek, and O. Edfors. "The Potential of Using Large Antenna Arrays on Intelligent Surfaces". In: *2017 IEEE 85th Vehicular Technology Conference (VTC Spring)*. 2017, pp. 1–6. DOI: 10.1109/VTCSpring.2017.8108330 (cit. on pp. 8, 19).

[15] S. Hu et al. "User Assignment with Distributed Large Intelligent Surface (LIS) Systems". In: *2018 IEEE 29th Annual International Symposium on Personal, Indoor and Mobile Radio Communications (PIMRC)*. 2018, pp. 1–6. DOI: 10.1109/PIMRC.2018.8580675 (cit. on pp. 8, 9, 19).

[16] S. Hu, F. Rusek, and O. Edfors. "Capacity Degradation with Modeling Hardware Impairment in Large Intelligent Surface". In: *2018 IEEE Global Communications Conference (GLOBECOM)* (2018), pp. 1–6 (cit. on p. 19).

[17] A. Im et al. "Angle of arrival estimation using MIMO array antenna". In: *2013 MTS/IEEE OCEANS - Bergen*. 2013, pp. 1–4. DOI: 10.1109/OCEANS-Bergen.2013.6607981 (cit. on p. 25).

[18] G. Interdonato et al. "Ubiquitous Cell-Free Massive MIMO Communications". In: *EURASIP Journal on Wireless Communications and Networking* (Aug. 2019). DOI: 10.1186/s13638-019-1507-0 (cit. on pp. 1, 9, 10).

[19] R. Jess-Williams, E. D. Carvalho, and T. Marzetta. "A Communication Model for Large Intelligent Surfaces". In: *2020 IEEE International Conference on Communications Workshops (ICC Workshops)* (2020), pp. 1–6 (cit. on pp. 8, 14).

[20] A. de Jesus Torres, L. Sanguinetti, and E. Björnson. *Near- and Far-Field Communications with Large Intelligent Surfaces*. 2020. arXiv: 2011.13835 [eess.SP] (cit. on pp. 8, 9, 13).

[21] M. Jung et al. "Performance Analysis of Large Intelligent Surfaces (LISs): Asymptotic Data Rate and Channel Hardening Effects". In: *IEEE Transactions on Wireless Communications* PP (Mar. 2020), pp. 1–1. DOI: 10.1109/TWC.2019.2961990 (cit. on pp. 8, 9, 14).

[22] A. Khansefid and H. Minn. "On Channel Estimation for Massive MIMO With Pilot Contamination". In: *IEEE Communications Letters* 19.9 (2015), pp. 1660–1663. DOI: 10.1109/LCOMM.2015.2452912 (cit. on p. 18).

[23] E. G. Larsson et al. "Massive MIMO for next generation wireless systems". In: *IEEE Communications Magazine* 52.2 (2014), pp. 186–195. DOI: 10.1109/MCOM.2014.6736761 (cit. on pp. 6, 16).

[24] Y. Li et al. "Exploiting Temporal Channel Correlation in Data-Assisted Massive MIMO Uplink Detection". In: *IEEE Communications Letters* 21.2 (2017), pp. 430–433. DOI: 10.1109/LCOMM.2016.2619341 (cit. on p. 18).

[25] C. Liaskos et al. "A New Wireless Communication Paradigm through Software-Controlled Metasurfaces". In: *IEEE Communications Magazine* 56.9 (2018), pp. 162–169. DOI: 10.1109/MCOM.2018.1700659 (cit. on p. 10).

[26] J. M. Lourenço. *The NOVAthesis LaTeX Template User's Manual*. NOVA University Lisbon. 2021. URL: https://github.com/joaomlourenco/novathesis/raw/master/template.pdf (cit. on p. ii).

[27] H. . Lu and Y. . Zeng. "Communicating with Extremely Large-Scale Array/Surface: Unified Modelling and Performance Analysis". In: *IEEE Transactions on Wireless Communications* (2021), pp. 1–1. DOI: 10.1109/twc.2021.3126384 (cit. on pp. 12, 13).

[28] T. L. Marzetta et al. *Fundamentals of Massive MIMO*. First. Cambridge University Press, 2016. ISBN: 978-1-107-17557-0 (cit. on pp. 1, 5–8, 15–17, 25).

[29] H. Ngo. *Massive MIMO: Fundamentals and System Designs*. Linköping Studies in Science and Technology. Dissertations. Linköping University Electronic Press, 2015. ISBN: 9789175191478. URL: https://books.google.pt/books?id=wiGKBwAAQBAJ (cit. on pp. 1, 5–8, 15–17, 25).

[30] A. Pereira et al. "On the Complexity Requirements of a Panel-Based Large Intelligent Surface". In: *GLOBECOM 2020 - 2020 IEEE Global Communications Conference*. 2020, pp. 1–6. DOI: 10.1109/GLOBECOM42002.2020.9347953 (cit. on p. 19).

[31] Z. H. Shaik, E. Björnson, and E. G. Larsson. "Cell-Free Massive MIMO with Radio Stripes and Sequential Uplink Processing". In: *2020 IEEE International Conference on Communications Workshops (ICC Workshops)*. 2020, pp. 1–6. DOI: 10.1109/ICCWorkshops49005.2020.9145164 (cit. on p. 10).

[32] C. Soni and N. Gupta. "Channel Estimation of Spatial Correlated Channel in Massive MIMO". In: *2021 8th International Conference on Computing for Sustainable Global Development (INDIACom)*. 2021, pp. 836–841 (cit. on p. 17).

[33] T. Wang et al. "Two-Dimension Direction-of-Arrival Estimation for Massive MIMO Systems". In: *IEEE Access* 3 (2015), pp. 2122–2128. DOI: 10.1109/ACCESS.2015.2496944 (cit. on p. 25).

[34] H. Wragg. "The Method of Geometric Optics and it's application to High Frequency Wave Propagation." English. In: SciCADE 2017 ; Conference date: 11-09-2017 Through 15-09-2017. Sept. 2017 (cit. on p. 21).

[35] Q. Wu and R. Zhang. "Towards Smart and Reconfigurable Environment: Intelligent Reflecting Surface Aided Wireless Network". In: *IEEE Communications Magazine* 58.1 (2020), pp. 106–112. DOI: 10.1109/MCOM.001.1900107 (cit. on p. 11).

[36] Z. Yun and M. F. Iskander. "Ray Tracing for Radio Propagation Modeling: Principles and Applications". In: *IEEE Access* 3 (2015), pp. 1089–1100. DOI: 10.1109/ACCESS.2015.2453991 (cit. on p. 21).